Multi-Waveform
Space-Time Adaptive Processing

Shannon D. Blunt[1], *IEEE Fellow,* Justin Metcalf [2], *IEEE Member,*
John Jakabosky[1,3], *IEEE Member,* James Stiles[1], *IEEE Senior Member,*
Braham Himed[2], *IEEE Fellow*

This work was supported in part by a subcontract with Booz, Allen and Hamilton for research sponsored by the Air Force Research Laboratory (AFRL) under Contract FA8650-11-D-1011. Portions were presented at the 2013 IEEE Radar Conference [1] and the 2014 IEEE International Radar Conference [2].

[1] Electrical Engineering & Computer Science Dept., Radar Systems & Remote Sensing Lab, University of Kansas, Lawrence, KS.

[2] Sensors Directorate - Air Force Research Laboratory, Wright-Patterson AFB, Dayton, OH.

[3] Radar Division - Naval Research Laboratory, Washington, DC.

Abstract

A new form of Space-Time Adaptive Processing (STAP) is presented that leverages additional training data obtained from waveform-diverse pulse compression filters possessing low cross-correlation with the primary waveform that is used for traditional airborne and space-based Ground Moving Target Indication (GMTI). In contrast to traditional training data in which clutter and targets are "focused" in range via pulse compression of the primary waveform, this new set of training data possesses a "smeared" range response that better approximates the *identically distributed* assumption made during sample covariance estimation. The Multi-Waveform STAP (MuW-STAP or simply μ-STAP) formulation is shown for both Multiple-Input Multiple-Output (MIMO) and Single-Input Multiple-Output (SIMO) configurations, with the former retaining the spatially-focused primary emission supplemented by low-power secondary emissions that illuminate sidelobe clutter and the latter a special case of the former. In simulation, Signal to Interference plus Noise Ratio (SINR) analysis reveals enhanced robustness to non-stationary interference compared to standard STAP training data.

Keywords

STAP, MIMO radar, airborne/space-based GMTI, non-homogeneous clutter

I. Introduction

Radar ground moving target indication (GMTI) from an airborne/space-based platform requires the use of a coupled space-time receive filter to cancel clutter effectively. In general, space-time adaptive processing (STAP) schemes determine this receive filter by estimating the covariance matrix of the clutter for a given cell-under-test (CUT), within which a target may also exist [3,4]. Ideally, estimation of the clutter covariance matrix employs target-free training data whose space-time characteristics are otherwise homogenous with that of the CUT. However, due to the tendency for clutter to be non-homogeneous in range and azimuth, the presence of internal clutter motion, the possible contamination of training data by targets of interest, and often insufficient sample support, the accurate estimation of the clutter covariance matrix remains one of the most difficult aspects of a practical STAP implementation [5-7]. To provide an additional tool to address this issue a new source of training data is proposed that is obtained from multiple waveform-diverse pulse compression filters designed to possess an unfocused response to the emitted *primary* waveform. Both multiple-input multiple output (MIMO) and single-input multiple-output (SIMO) arrangements are considered and their relative merits and trade-offs discussed. It is anticipated that this new training data may be leveraged to further enhance existing robust STAP implementations.

The spatial and slow-time (Doppler) channels provided respectively by N antenna elements and M pulses in the coherent processing interval (CPI) clearly establish a multi-channel framework for interference suppression and subsequent target detection. That said, standard GMTI STAP is conventionally viewed as a single-input single-output (SISO) operation due to the emission and subsequent receiver pulse compression of a single waveform. This emitted waveform illuminates the clutter and targets according to the transmit spatial beampattern, with Doppler induced by the motion of the platform, radial target motion, and intrinsic clutter motion. In general, estimation of the STAP covariance matrix $\mathbf{R}(\ell_{\text{CUT}})$, representing a second-order characterization of clutter and other interference within the CUT range cell, is realized as [4]

$$\hat{\mathbf{R}}(\ell_{\text{CUT}}) = \frac{1}{n(L)} \sum_{\substack{\ell \in L \\ \ell \neq \ell_{\text{CUT}}}} \mathbf{z}(\ell)\, \mathbf{z}^{H}(\ell) + \sigma_v^2 \mathbf{I}\,, \tag{1}$$

using the $n(L)$ space-time training data snapshots $\mathbf{z}(\ell)$ in set L that are near the CUT according to range index ℓ. The CUT snapshot and guard cells are generally excluded to avoid self-cancellation of a prospective target in the CUT. Diagonal loading by the noise power σ_v^2, which can be readily estimated in practice since the receiver thermal noise dominates external noise at microwave frequencies [8], alleviates some of the numerical problems of low sample support.

Under the condition that the interference is independent and identically distributed (i.i.d.), the training data is homogeneous with the interference in the CUT. Thus, the well-known rule of Reed, Mallet, and Brennan applies, which states that $\hat{\mathbf{R}}(\ell_{\mathrm{CUT}})$ yields a signal to interference plus noise ratio (SINR) that is within 3 dB of optimal if the number of snapshots $n(L)$ is at least $2NM-3$ [9], notwithstanding the use of reduce-rank processing (see [3]) that exploits the fact that clutter is typically not full rank. This minimum number increases when the training data is non-homogeneous [5-7], thus leading to insufficient sample support for accurate interference characterization that subsequently results in increased false alarms and/or degraded detection sensitivity. Numerous robust methods have been developed to address these practical limitations (e.g. [7,8,10-30], references therein, and many others) using techniques such as non-homogeneity detection, *a priori* knowledge, statistical modeling, imposing matrix structure, etc. with varying degrees of enhanced robustness, computational requirements, and necessary assumptions.

The fundamental problem introduced by non-homogeneous interference is that, while the training data samples may be statistically independent, they are not identically distributed. In such a case, the Sample Covariance Matrix (SCM) in (1) is a poor estimate of the true interference covariance matrix corresponding to $\mathbf{z}(\ell_{\text{CUT}})$, thus resulting in under/over-nulled interference that degrades detection performance. For example, a clutter discrete (such as induced by a building, water tower, etc.) will often generate a response at the radar receiver that is larger than the surrounding clutter. When a large discrete is present in the CUT, it therefore cannot be adequately suppressed using the SCM that is based on the surrounding clutter that does not include the CUT.

Clearly, knowledge of such non-homogeneities in the CUT needs to be incorporated into the SCM, yet direct inclusion of $\mathbf{z}(\ell_{\text{CUT}})$ in the SCM estimation of (1) could likewise suppress a prospective target that may reside in the CUT. This conundrum exemplifies the practical difficulty encountered with STAP [31]. A prominent notion that has been examined in recent years is to exploit prior knowledge of the clutter as a means to better model the interference in the CUT (e.g. [25-28]). Another approach is to select an appropriate subset of the training data (i.e. non-homogeneity detection) while including some portion of $\mathbf{z}(\ell_{\text{CUT}})$ in the SCM [12-15,19] by relying on the fact that the targets we seek to detect using STAP are generally received with powers far below that of the clutter (or else STAP would not be needed). Thus the problem becomes one of selection of appropriate training data followed by appropriate scaling of snapshots to minimize contamination by targets of interest that would otherwise induce self-cancellation.

Here, we take a step back (from a processing chain perspective) to consider the impact that pulse compression has on STAP covariance estimation and how an expansion of the pulse compression process using waveform diversity [32-35] could be used to provide additional useful training data for subsequent robust covariance matrix estimation, such as via the techniques denoted above. Specifically, additional *secondary* pulse compression filters are incorporated in parallel to the receive filter corresponding to the *primary* waveform, where the waveforms to which these secondary filters are matched exhibit a low cross-correlation with the primary waveform. These secondary filters yield a range-smeared response to the echoes generated by the primary waveform, and thereby intrinsically capture the non-homogeneities in range (such as clutter discretes) while inherently de-emphasizing the already small target echoes to avoid self-cancellation. This smearing by the secondary filters provides a "homogenization" in the range dimension that validates the *identically distributed* assumption. Of course, as will be demonstrated, this range-domain form of linear pre-processing does not introduce new independent training data.

This waveform-diverse manner of training data generation can be performed as a SIMO mode for existing GMTI systems or as a MIMO mode whereby a small amount of primary mainbeam power is diverted to emit the secondary waveform(s) in the spatial directions corresponding to the sidelobes of the primary mainbeam. The inherent trade-off for the MIMO mode is the degree of lost primary mainbeam SNR (for target detection in mainbeam clutter) to provide power for the secondary emission(s). It is important to note that no assumptions regarding the statistical or structural properties of the interference are required to obtain the Multi-Waveform STAP training data (which we shall refer to as MuW-STAP, or simply μ-STAP).

II. Multi-Waveform STAP

Classifying standard STAP as a single-input single-output (SISO) configuration, since it involves the use of only one waveform, the MIMO version is clearly an expansion to the emission and subsequent reception of multiple waveforms (though not with equal transmit power if it is to be useful for GMTI). The SIMO version is then a special case of MIMO in which the standard single waveform is emitted, yet multiple waveform-oriented receive filters are still applied to obtain additional diverse receive channels of training data. We begin by establishing the standard SISO framework and then generalize to the MIMO and SIMO cases.

A) Standard SISO STAP

Consider the standard STAP formulation for an airborne/space-based GMTI radar with N antenna elements in a uniform linear array that transmit a coherent processing interval (CPI) of M pulses modulated with waveform $s(t)$ in the spatial look direction θ_{look}. This waveform is physically realizable using a power-efficient transmitter and is designed according to the usual criteria of low range sidelobes and perhaps Doppler tolerance (e.g. [36,37]). This well-known SISO STAP architecture involves the collection of the resulting echoes to perform adaptive processing and subsequently attempt to discern moving targets. This received signal can be defined as

$$y(m,n,t) = \sum_{\omega}\sum_{\theta}\left[\tilde{s}(t,\theta,\theta_{\text{look}}) * x(t,\theta,\omega)\right]e^{j(m\omega+n\theta)} + v_{\text{noise}}(t) + v_{\text{jam}}(t), \qquad (2)$$

where $\tilde{s}(t,\theta,\theta_{\text{look}}) = s(t)\,b(\theta,\theta_{\text{look}})$, for $b(\theta,\theta_{\text{look}})$ the transmit beampattern relative to look direction θ_{look} that illuminates the scatterers in $x(t,\theta,\omega)$ as a function of spatial angle θ and Doppler frequency ω, the operation $*$ is convolution, $v_{\text{noise}}(t)$ is additive noise, and $v_{\text{jam}}(t)$ is noise-like barrage jamming [3,4]. The summations in (2) collect the clutter (and possible target responses) that are distributed over angle and Doppler.

The first processing stage for the received signal of (2) is to perform pulse compression, which can be written as

$$z(m,n,t) = h(t) * y(m,n,t)\,, \tag{3}$$

for $h(t)$ a matched or mismatched filter of waveform $s(t)$. Regardless of whether pulse compression is performed in analog (with sampling to follow) or digitally, a discretized version of (3) is obtained that is represented as $z(m,n,\ell)$, where ℓ is the discrete range index. We shall assume throughout that the pulse compression filter is normalized to produce a unity response at the matched point (or very close to unity in the case of mismatch filtering).

For a uniform linear array the spatial steering vector for direction θ is formed as

$$\mathbf{c}_{\text{s}}(\theta) = [1\ \ \exp(j\theta)\ \ \exp(j2\theta)\ \ \cdots\ \ \exp(j(N\!-\!1)\theta)]^T\,. \tag{4}$$

Likewise, for Doppler frequency ω_{D} a temporal steering vector is formed as

$$\mathbf{c}_{\text{t}}(\omega_{\text{D}}) = [1\ \ \exp(j\omega_{\text{D}})\ \ \exp(j2\omega_{\text{D}})\ \ \cdots\ \ \exp(j(M\!-\!1)\,\omega_{\text{D}})]^T\,. \tag{5}$$

The space-time steering vector for specific direction θ = θ_{look} and arbitrary ω_{D} is therefore

$$\mathbf{c}_{\text{st}}(\theta_{\text{look}}, \omega_{\text{D}}) = \mathbf{c}_{\text{t}}(\omega_{\text{D}}) \otimes \mathbf{c}_{\text{s}}(\theta_{\text{look}})\,, \tag{6}$$

where $\otimes$ is the Kronecker product. The discretized pulse compressed outputs from (3) are organized in the same manner as the space-time steering vector of (6) to yield length-NM space-time snapshots denoted as $\mathbf{z}(\ell)$. These snapshots represent the primary data and can be used to obtain the estimated CUT interference SCM denoted as $\hat{\mathbf{R}}(\ell_{\text{CUT}})$ via (1) to form the standard (SISO) STAP filter as

$$\mathbf{w}(\ell_{\text{CUT}},\theta_{\text{look}},\omega_D) = \hat{\mathbf{R}}^{-1}(\ell_{\text{CUT}})\ \mathbf{c}_{\text{st}}(\theta_{\text{look}},\omega_D)\,, \tag{7}$$

for application to the CUT snapshot as

$$\alpha(\ell_{\text{CUT}},\omega_D) = \mathbf{w}^H(\ell_{\text{CUT}},\theta_{\text{look}},\omega_D)\ \mathbf{z}(\ell_{\text{CUT}})\,. \tag{8}$$

The resulting value $\alpha(\ell_{\text{CUT}},\omega_D)$ is then compared to a threshold (e.g. generated via CFAR detector [38]) to ascertain the presence of a target in range and Doppler. Of course, practical effects such as non-homogeneous clutter, discretes, and contaminating targets necessitate this primary training data be employed within more robust implementations of (1), such as via [7,8,10-30].

Now consider how waveform diversity could be employed to supplement this primary training data with additional secondary training data that could likewise be incorporated into the various robust STAP implementations. In so doing it is important to note that a generalization to MIMO is only useful to the degree that it enhances the practical performance of STAP without the requirement of additional assumptions such as orthogonality, perfect knowledge of the clutter distribution or array manifold, etc. [31,39].

B) Practical MIMO for STAP

To date, the practical application of MIMO to radar has been largely limited to over-the-horizon (OTH) radar (e.g. [40,41]) and as a means to synchronize spatially distributed transmitters to "cohere-on-target" [42]. For GMTI, the oft-proposed MIMO trade-off between spatial directivity and dwell time is unlikely to be feasible in many circumstances due to short decoherence time and “range walking” effects for moving targets [39]. As such, the benefit of the usual focused mainbeam must be balanced against the possible diversity afforded by emitting multiple waveforms. Further, any transmitted waveforms must be physically realizable and therefore must be continuous, relatively bandlimited signals that are amenable to a physical transmitter [36,37,39]. Finally, given the feasible (non-zero) cross-correlation that can be achieved for a set of physical waveforms occupying the same spectrum with respect to the high dynamic range of the received clutter, targets, and noise powers, the mathematical assumption of waveform “orthogonality” is not appropriate (and also compounded by the fact that clutter is distributed in range and angle).

These requirements as well as other physical constraints lead to a set of practical attributes for a MIMO GMTI radar that are summarized in Table I. Given a finite power source, the loss of power to the focused mainbeam due to the concurrent emission of additional waveforms involves a trade-off between energy on target (detection probability) and any diversity-induced enhancement to clutter suppression that may be achieved. Likewise, power efficiency necessitates operation of power amplifiers in saturation, which requires constant modulus, relatively bandlimited waveforms to minimize transmitter distortion. Lastly, simultaneously emitting different waveforms from the different antenna elements within an array can be significantly impacted by imperfect array calibration and mutual coupling between elements [43,44], which suggests instead that sub-arraying or even separate antennas be used to generate the different waveforms, though such separation may introduce further practical issues to consider that are not addressed here.

TABLE I. PRACTICAL ASPECTS FOR MIMO GMTI

1) Avoid loss of spatial resolution (maintain focused mainbeam)
2) Minimize loss of mainbeam power (minimize detection loss)
3) Physical emissions (continuous, relatively bandlimited waveforms)
4) Constant modulus waveforms for high power emissions
5) Non-zero waveform cross-correlation (not orthogonal)
6) Non-ideal antenna arrays (calibration, mutual coupling, arrangement on platform)

With this litany of practical constraints in mind, we propose a pragmatic approach to incorporating MIMO into airborne/space-based GMTI for the purpose of improving suppression of sidelobe clutter, to subsequently enhance target detection and reduce false alarms, while maintaining the objective of cancelling mainlobe clutter that obfuscates moving targets. Denote the original GMTI waveform from (2) as the *primary* waveform and label it as $s_{\text{prime}}(t)$. This waveform is to be emitted as usual for GMTI using a high-power focused beam in spatial direction θ_{look}. In addition, assuming the presence of K separate sub-arrays and/or antennas on the same platform, K secondary waveforms denoted as $s_{\text{sec},k}(t)$ for $k=1,2,\cdots,K$ are simultaneously transmitted with the stipulations that 1) they emit minimal power in spatial direction θ_{look} that corresponds to the primary mainbeam and 2) they are designed to have minimal cross-correlation with the primary waveform (though not necessarily with one another). As such, the primary mainbeam emission and the secondary emissions are separable in both the waveform (range) and spatial domains. Further, these secondary waveforms are emitted at a much lower power than the primary to minimize the amount of power diverted from the primary mainbeam, which still performs the traditional STAP function of clutter cancellation for subsequent target detection in direction θ_{look}.

Given this MIMO emission scenario, the received signal from (2) is now expanded as

$$
\begin{aligned}
y(m,n,t) = &\sum_{\omega}\sum_{\theta}\left[\tilde{s}_{\text{prime}}(t,\theta,\theta_{\text{look}}) * x(t,\theta,\omega)\right]e^{j(m\omega+n\theta)} \\
&+\sum_{k=1}^{K}\sum_{\omega}\sum_{\theta}\left[\tilde{s}_{\text{sec},k}(t,\theta,\theta_{\text{look}}) * x(t,\theta,\omega)\right]e^{j(m\omega+n\theta)}\,, \\
&+v_{\text{noise}}(t) + v_{\text{jam}}(t)
\end{aligned}
\tag{9}
$$

where $\tilde{s}_{\text{prime}}(t,\theta,\theta_{\text{look}}) = s_{\text{prime}}(t)\ b_{\text{prime}}(\theta,\theta_{\text{look}})$, for $b_{\text{prime}}(\theta,\theta_{\text{look}})$ the primary transmit beampattern relative to θ_{look}, illuminates $x(t,\theta,\omega)$ as a function of angle θ and Doppler ω. Likewise, the kth secondary emission $\tilde{s}_{\text{sec},k}(t,\theta,\theta_{\text{look}}) = s_{\text{sec},k}(t)\ b_{\text{sec},k}(\theta,\theta_{\text{look}})$, for $b_{\text{sec},k}(\theta,\theta_{\text{look}})$ the kth secondary transmit beampattern relative to θ_{look} (with low power in the θ_{look} direction), illuminates $x(t,\theta,\omega)$ as a function of angle and Doppler, for $k = 1, 2, \cdots, K$. It is useful at this point to rewrite (9) so that the beampattern is associated with the scattering response instead of the transmitted waveform as

$$
\begin{aligned}
y(m,n,t) = &\sum_{\omega}\sum_{\theta}\left[s_{\text{prime}}(t) * \tilde{x}_{\text{prime}}(t,\theta,\omega,\theta_{\text{look}})\right]e^{j(m\omega+n\theta)} \\
&+\sum_{k=1}^{K}\sum_{\omega}\sum_{\theta}\left[s_{\text{sec},k}(t) * \tilde{x}_{\text{sec},k}(t,\theta,\omega,\theta_{\text{look}})\right]e^{j(m\omega+n\theta)}\,, \\
&+v_{\text{noise}}(t) + v_{\text{jam}}(t)
\end{aligned}
\tag{10}
$$

where $\tilde{x}_{\text{prime}}(t,\theta,\omega,\theta_{\text{look}}) = x_{\text{prime}}(t,\theta,\omega)\ b_{\text{prime}}(\theta,\theta_{\text{look}})$ is the response to the primary beampattern, for which the mainbeam points in direction θ_{look}, and $\tilde{x}_{\text{sec},k}(t,\theta,\omega,\theta_{\text{look}}) = x_{\text{sec},k}(t,\theta,\omega)\ b_{\text{sec},k}(\theta,\theta_{\text{look}})$ is the response to each of the K secondary beampatterns, each of which de-emphasizes the scattering in direction θ_{look}. Assuming the total $K+1$ waveforms are all constant modulus, the relative instantaneous powers of their associated emissions are

$$P_{\text{prime}} = \int_{\theta} \left| b_{\text{prime}}(\theta, \theta_{\text{look}}) \right|^2 d\theta \tag{11}$$

and

$$P_{\text{sec},k} = \int_{\theta} \left| b_{\text{sec},k}(\theta, \theta_{\text{look}}) \right|^2 d\theta \quad \text{for} \quad k = 1, 2, \cdots, K\,, \tag{12}$$

resulting in the total emitted power

$$P_{\text{total}} = P_{\text{prime}} + \sum_{k=1}^{K} P_{\text{sec},k}\,, \tag{13}$$

which is a constant regardless of how power is distributed among the $K+1$ emissions.

As with the standard SISO STAP formulation, the first processing stage for the received signal in (10) is pulse compression. The bank of filters corresponding to the $K+1$ emitted waveforms is applied as

$$\begin{aligned} z_{\text{prime}}(m,n,t) &= h_{\text{prime}}(t) * y(m,n,t) \\ z_{\text{sec},1}(m,n,t) &= h_{\text{sec},1}(t) * y(m,n,t) \\ &\vdots \\ z_{\text{sec},K}(m,n,t) &= h_{\text{sec},K}(t) * y(m,n,t) \end{aligned}\,, \tag{14}$$

where $h_{\text{prime}}(t)$ is the primary pulse compression filter corresponding to $s_{\text{prime}}(t)$ and $h_{\text{sec},i}(t)$ for $i = 1, 2, \cdots, K$ is the pulse compression filter corresponding to the ith secondary waveform. Using index 0 to denote the primary waveform/filter for compactness, the set of $K+1$ filter outputs from (14) can thus be combined with the received signal representation of (10) as

$$\begin{aligned} z_i(m,n,t) &= \sum_{k=0}^{K} \sum_{\omega} \sum_{\theta} \left[a_{k,i}(t) * \tilde{x}_k(t, \theta, \omega, \theta_{\text{look}}) \right] e^{j(m\omega + n\theta)} \\ &\quad + \overline{v}_{\text{noise},i}(t) + \overline{v}_{\text{jam},i}(t) \end{aligned} \quad \text{for} \quad i = 0, 1, 2, \cdots, K\,, \tag{15}$$

in which $a_{k,i}(t) = h_i(t) * s_k(t)$ is the filter response to each of the $K+1$ waveforms, and $\bar{v}_{\text{noise},i}(t)$ and $\bar{v}_{\text{jam},i}(t)$ are the *i*th filter responses to noise and jamming, respectively. The components in (15) for which $i = k$ correspond to a range-focused response due to coherent integration while the components for which $i \neq k$ produce a range smearing of the associated echo response $\tilde{x}_k(t, \theta, \omega, \theta_{\text{look}})$ that provides a useful homogenizing effect on the interference that is non-homogeneous in range. As with the SISO case, the filtered outputs are discretized and collected in like manner to the space-time steering vector in (6) to realize the snapshots $\mathbf{z}_{\text{prime}}(\ell)$ and $\mathbf{z}_{\text{sec},i}(\ell)$ for $i = 1, 2, \cdots, K$.

Considering (15), with the ultimate goal of isolating the target echoes in look direction θ_{look} for Doppler frequencies ω_{D} parameterized by (5), it is evident that the emissions should be designed according to two criteria. First, in addition to the usual design considerations for the primary waveform (e.g. low range sidelobes, Doppler tolerance) the secondary waveform should be designed such that

$$\min_{s_{\text{sec},k}(t)} \max_{\tau} \left| \int s_{\text{prime}}(t)\, s^*_{\text{sec},k}(t+\tau)\, dt \right|^2 \quad \forall k \tag{16}$$

to minimize the peak cross-correlation between the primary waveform and each of the secondary waveforms so that the associated filter responses $a_{k,i}(t)$ in (15) provide some degree of separability in the waveform (range) domain. Because the cross-correlation response is in fact useful as a means to aggregate the interference in range, these secondary waveforms are constrained to be constant modulus and generally possess the same spectral footprint as the primary. Further, for the MIMO instantiation the secondary waveforms must likewise adhere to the physical design requirements from Table I (e.g. via [36,37]).

The second emission design goal is that

$$b_{\text{prime}}(\theta=\theta_{\text{look}},\theta_{\text{look}}) \gg b_{\text{sec},k}(\theta=\theta_{\text{look}},\theta_{\text{look}}) \quad \forall k\,, \tag{17}$$

to either optimize or constrain the primary response to be much greater than the secondary responses in the look direction of the radar. This requirement provides separability of the primary and secondary responses in the spatial domain (at least in the look direction). As with the need for physical waveforms, these beampatterns are likewise limited to what can be physically achieved within the context of mutual coupling and non-ideal calibration.

For example, Fig. 1 illustrates the primary and four secondary matched filter responses (per (16)) to an optimized primary waveform (implemented via the polyphase-coded FM (PCFM) framework of [36,37] and having time-bandwidth product of 100). Where the primary (auto-correlation) response is focused in range, the secondary (cross-correlation) responses are smeared in range with different sidelobe structures. Likewise, Fig. 2 depicts the standard primary beampattern (with θ_{look} at boresight) and a possible secondary beampattern that is omnidirectional (per (17)).

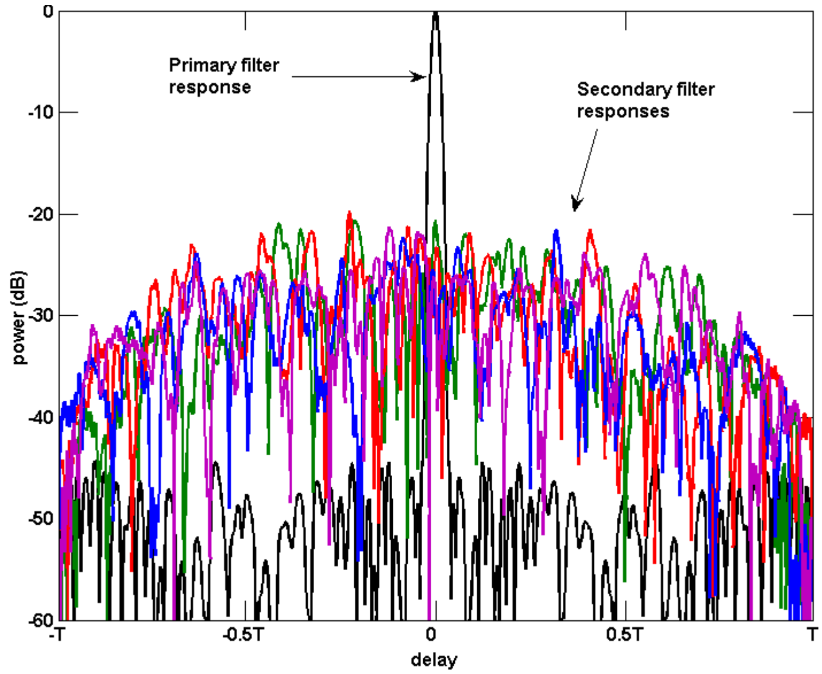

Fig. 1: Primary and secondary matched filter responses to an optimized primary waveform with $BT = 100$

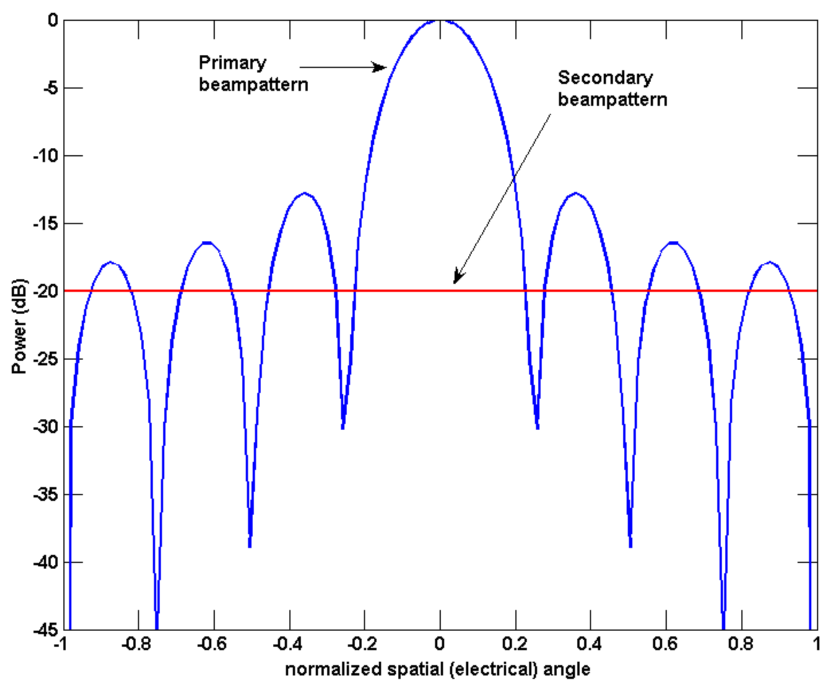

Fig. 2: Primary beampattern (for $N = 8$ antenna elements) and an omnidirectional secondary beampattern

The K secondary filter outputs in (14) and (15) represent a new source of STAP training data that provide a diverse perspective on the collective interference response by virtue of the waveform and spatial separability between the primary and secondary emissions with respect to the look direction. We denote this new training data formulation as Multi-Waveform (MuW) STAP, or simply μ-STAP.

Leveraging the new training data, the baseline sample covariance matrix (SCM) of (1) can be modified in a couple different ways. First, a new SCM can be defined by supplementing (1) with secondary training data as

$$\begin{aligned}\hat{\mathbf{R}}_{\mu}(\ell_{\mathrm{CUT}}) = & \frac{1}{n(L_{\mathrm{prime}})} \sum_{\substack{\ell \in L_{\mathrm{prime}} \\ \ell \neq \ell_{\mathrm{CUT}}}} \mathbf{z}_{\mathrm{prime}}(\ell)\, \mathbf{z}^{H}_{\mathrm{prime}}(\ell) \\ & + \frac{1}{n(L_{\mathrm{sec}})\,K} \sum_{i=1}^{K} \sum_{\ell \in L_{\mathrm{sec}}} \mathbf{z}_{\mathrm{sec},i}(\ell)\, \mathbf{z}^{H}_{\mathrm{sec},i}(\ell) \\ & + \sigma_v^2 \mathbf{I} \\ = & \; \hat{\mathbf{R}}_{\mathrm{prime}}(\ell_{\mathrm{CUT}}) + \frac{1}{K}\sum_{i=1}^{K} \hat{\mathbf{R}}_{\mathrm{sec},i}(\ell_{\mathrm{CUT}}) + \sigma_v^2 \mathbf{I}\end{aligned} \quad . \tag{18}$$

Here $n(L_{\mathrm{prime}})$ is the cardinality of the set L_{prime} for the primary data snapshots which excludes the CUT and guard cells, while $n(L_{\mathrm{sec}})$ is the cardinality of the set L_{sec} for the secondary data snapshots that, in contrast, can contain the CUT and surrounding guard cells. The inclusion of the CUT and guard cells in the secondary training data is valid because of the separability achieved through proper waveform and beampattern design via (16) and (17) that serves to diminish the relative power of mainbeam targets of interest (generally of lower power) within the secondary data while also capturing the specific interference (typically of much higher power) present in the CUT. By using (18) to replace the SCM in (7), the μ-STAP filter is formed.

Alternatively, the secondary training data could be used without the primary as

$$\begin{aligned}\hat{\mathbf{R}}_{\mu,\mathrm{NP}}(\ell_{\mathrm{CUT}}) &= \frac{1}{n(L_{\mathrm{sec}})\,K}\sum_{i=1}^{K}\sum_{\ell\in L_{\mathrm{sec}}}\mathbf{z}_{\mathrm{sec},i}(\ell)\,\mathbf{z}_{\mathrm{sec},i}^{H}(\ell) + \sigma_v^2\mathbf{I} \\ &= \frac{1}{K}\sum_{i=1}^{K}\hat{\mathbf{R}}_{\mathrm{sec},i}(\ell_{\mathrm{CUT}}) + \sigma_v^2\mathbf{I}\end{aligned}, \qquad (19)$$

where the subscript 'NP' denotes *no primary* data is used. Likewise, using (19) to replace the SCM in (7) results in a version of the μ-STAP filter that is based only on the secondary training data. Note that the primary data portion of the SCM in (18) is not scaled with respect to the number of additional secondary training data sets *K*. If it were, then increasing *K* would simply converge towards the NP version in (19). Here we shall address the two SCM forms in (18) and (19), though whether there is an optimum scaling among the various primary and secondary components remains an open question (the analysis in Section III may shed further light on the matter). Of course, such an optimality condition is likely to be an intrinsic function of the echo responses $\mathbf{z}_{\mathrm{prime}}$ and $\mathbf{z}_{\mathrm{sec},i}$ for $i = 1, 2, \cdots, K$, which are not known a priori.

It is worth mentioning that, even though it does not use the primary training data, the SCM in (19) is capable of cancelling mainbeam clutter despite the secondary emissions having transmit beampatterns with little/no gain in direction θ_{look}. The reason for this effect is that the primary waveform / secondary filter cross-correlations in (14) and (15), and exemplified in Fig. 1, still serve to capture the mainbeam clutter response. Further, while not considered here, robust STAP processors (e.g. [7,8,10-30]) such as data-adaptive censoring/scaling of training data could likewise be extended to incorporate this new secondary training data.

C) SIMO μ-STAP

The SIMO instantiation of the μ-STAP formulation is essentially a special case of the MIMO version in which $P_{\text{sec},k} = 0$ for $k = 1, 2, \cdots, K$. In other words, only the primary waveform is actually emitted which, without the need to divert power to transmit the secondary waveform(s), therefore achieves the maximum mainbeam power and thus the maximum receive SNR for any illuminated targets in the mainbeam. From a transmit perspective, the SIMO formulation is identical to the standard SISO framework.

For the SIMO case, the received signal from (9) and (10) now becomes

$$\begin{aligned} y(m,n,t) &= \sum_{\omega}\sum_{\theta}\left[\tilde{s}_{\text{prime}}(t,\theta,\theta_{\text{look}}) * x(t,\theta,\omega)\right]e^{j(m\omega+n\theta)} \\ &\quad + v_{\text{noise}}(t) + v_{\text{jam}}(t) \\ &= \sum_{\omega}\sum_{\theta}\left[s_{\text{prime}}(t) * \tilde{x}_{\text{prime}}(t,\theta,\omega,\theta_{\text{look}})\right]e^{j(m\omega+n\theta)} \\ &\quad + v_{\text{noise}}(t) + v_{\text{jam}}(t) \end{aligned}, \tag{20}$$

which is the response to the primary emission alone (i.e. same as the SISO case). However, the bank of filters from (14) is still applied so that the filter outputs from (15), again using index 0 to denote the primary waveform/filter for compactness, now yield

$$\begin{aligned} z_i(m,n,t) &= \sum_{\omega}\sum_{\theta}\left[a_{0,i}(t) * \tilde{x}_0(t,\theta,\omega,\theta_{\text{look}})\right]e^{j(m\omega+n\theta)} \\ &\quad + \overline{v}_{\text{noise},i}(t) + \overline{v}_{\text{jam},i}(t) \end{aligned} \quad \text{for} \;\; i = 0, 1, 2, \cdots, K. \tag{21}$$

Thus, the secondary filter outputs consist only of range-smeared versions of the echoes generated by the primary emission, thereby still providing homogenized secondary training data to implement SCM estimation via (18) or (19), albeit without the loss of primary mainbeam power otherwise needed to generate secondary MIMO emissions.

It is interesting to note that the SIMO μ-STAP approach bears some similarity to the notion of a data-adaptive de-emphasis factor as described in [12-15,19] in so far as the unfocused secondary data provides much less signal gain on any single range cell such that targets in the secondary training data produce little self-cancellation degradation (though those previous approaches focused on how to modify the existing sample data, whereas μ-STAP non-adaptively produces additional sets of training data). Likewise, SIMO μ-STAP can also be viewed as being related to multi-resolution STAP approaches such as those in [45,46] that leverage high-resolution SAR imaging to generate low-resolution GMTI training data (the analogy to μ-STAP is the range smearing of training data via the cross-correlation of the primary waveform and the secondary filters as in Fig. 1).

III. Analysis of μ-STAP Covariance Estimation

Because it is not necessarily obvious that μ-STAP should provide a good estimate of the interference covariance matrix for the CUT, we analytically examine this covariance matrix under the condition of homogeneous clutter in noise. For simplicity we first restrict attention to the SIMO response of (21), comparing the resulting theoretical covariance matrix arising from secondary filtering to that based on primary filtering such as in the standard SISO case, and then likewise consider the MIMO response of (15). The impact of non-homogeneous interference is then examined relative to the homogenous cases as a result of primary and secondary SCM estimation as part of (18) and (19).

A) SIMO Covariance Matrix Analysis

Applying the ith matched filter to the received signal of (20) yields (21) which, after collecting the NM channels and using (6), can be expressed as

$$\begin{aligned}\mathbf{z}_i(t) &= \sum_{\omega}\sum_{\theta}\left[a_{0,i}(t) * \tilde{x}_0(t,\theta,\omega,\theta_{\text{look}})\right]\mathbf{c}_{\text{st}}(\theta,\omega) \\ &\quad + \bar{\mathbf{v}}_{\text{noise},i}(t) + \bar{\mathbf{v}}_{\text{jam},i}(t) \\ &= \sum_{\omega}\sum_{\theta} b_0(\theta,\theta_{\text{look}})\left[a_{0,i}(t) * x(t,\theta,\omega)\right]\mathbf{c}_{\text{st}}(\theta,\omega) \\ &\quad + \bar{\mathbf{v}}_{\text{noise},i}(t) + \bar{\mathbf{v}}_{\text{jam},i}(t)\end{aligned} \quad . \tag{22}$$

In the lower portion of (22) we have separated the primary transmit beampattern from the scattering and the bar above the noise and jamming terms indicate they have been filtered by $h_i(t)$.

Assuming stationarity, the SIMO space-time covariance matrix for (22) is

$$\mathbf{R}_i^{(\text{SIMO})} = E\left[\mathbf{z}_i(t)\ \mathbf{z}_i^H(t)\right], \tag{23}$$

which, for i =0, is identical to that for standard SISO STAP. Inserting (22) into (23) and assuming that every clutter patch is statistically independent (likewise for barrage jamming and noise) with no targets present, and taking the expectation, results in

$$\begin{aligned}\mathbf{R}_i^{(\text{SIMO})} &= \sum_{\omega}\sum_{\theta}\left|b_0(\theta,\theta_{\text{look}})\right|^2\left[\left|a_{0,i}(t)\right|^2 * E\left|x(t,\theta,\omega)\right|^2\right]\mathbf{c}_{\text{st}}(\theta,\omega)\,\mathbf{c}_{\text{st}}^H(\theta,\omega) \\ &\quad + \bar{\mathbf{R}}_{\text{noise},i} + \bar{\mathbf{R}}_{\text{jam},i}\end{aligned} \quad , \tag{24}$$

which simplifies to

$$\begin{aligned}\mathbf{R}_i^{(\text{SIMO})} &= \sum_{\omega}\sum_{\theta}\left[\left|b_0(\theta,\theta_{\text{look}})\right|^2 \sigma_{\text{clut}}^2(\theta,\omega)\int_{-T}^{T}\left|a_{0,i}(t)\right|^2 dt\right]\mathbf{c}_{\text{st}}(\theta,\omega)\,\mathbf{c}_{\text{st}}^H(\theta,\omega) \\ &\quad + \bar{\mathbf{R}}_{\text{noise}} + \bar{\mathbf{R}}_{\text{jam}}\end{aligned} \tag{25}$$

for pulsewidth T. In (25) the term

$$\sigma_{\text{clut}}^2(\theta,\omega) = E\left|x(t,\theta,\omega)\right|^2 \tag{26}$$

is the expected clutter power as a function of Doppler and angle (coupled due to platform motion), and the noise and jamming terms have been generalized as $\bar{\mathbf{R}}_{\text{noise},i} = \bar{\mathbf{R}}_{\text{noise}}$ and $\bar{\mathbf{R}}_{\text{jam},i} = \bar{\mathbf{R}}_{\text{jam}}$, respectively, since pulse compression would not affect their space-time properties.

For the primary receive filter (i = 0), the matched filter response $a_{0,0}(t)$ is generally designed to possess a narrow mainbeam (for the given time-bandwidth product) and low range sidelobes. Thus, it is typically assumed (e.g. [3]) that $a_{0,0}(t)$ can be replaced by an impulse function $\delta(t)$. In so doing, (25) further simplifies to the SISO covariance matrix

$$\begin{aligned} \mathbf{R}^{(\text{SISO})} &= \mathbf{R}_{i=0}^{(\text{SIMO})} \\ &= \sum_{\omega}\sum_{\theta}\left[\left|b_0(\theta,\theta_{\text{look}})\right|^2 \sigma_{\text{clut}}^2(\theta,\omega)\right]\mathbf{c}_{\text{st}}(\theta,\omega)\,\mathbf{c}_{\text{st}}^H(\theta,\omega)\,. \\ &\quad + \bar{\mathbf{R}}_{\text{noise}} + \bar{\mathbf{R}}_{\text{jam}} \end{aligned} \tag{27}$$

Note that the result in (27) is realized by setting

$$\int_{-T}^{T}\left|a_{0,0}(t)\right|^2 dt \cong \int_{-T}^{T}\left|\delta(t)\right|^2 dt = 1\,. \tag{28}$$

In contrast, the SIMO covariance matrix for the data produced by a secondary filter ($i \neq 0$) cannot be further simplified beyond (25) since the structure of the cross-correlation $a_{0,i}(t)$ is arbitrary. However, based on Monte Carlo trials using physical Frequency Modulated (FM) waveforms (derived from [36,37]) and shown in Appendix

A), it can be inferred that the final unity condition in (28) is relatively well approximated if the secondary matched filters correspond to waveforms possessing at least a modest time-bandwidth product (> 20, which is easily achieved) and possess the same physical traits as the primary waveform (i.e. constant modulus, continuous, well-contained spectrally, same pulsewidth). While the extent of design freedom for these secondary filters is still being explored, the above analysis demonstrates that their output provides a valid source of STAP training data, even when combined as in (18) and (19) since the relative scaling is small.

B) MIMO Covariance Matrix Analysis

For the MIMO emission scheme the data vector representation of (22) can be generalized using (15) as

$$\begin{aligned}\mathbf{z}_i(t) &= \sum_{k=0}^{K}\sum_{\omega}\sum_{\theta} b_k(\theta,\theta_{\text{look}})\left[a_{k,i}(t) * x(t,\theta,\omega)\right]\mathbf{c}_{\text{st}}(\theta,\omega) \\ &\qquad + \overline{\mathbf{v}}_{\text{noise},i}(t) + \overline{\mathbf{v}}_{\text{jam},i}(t) \\ &= \sum_{\omega}\sum_{\theta}\left[g_i(t,\theta,\theta_{\text{look}}) * x(t,\theta,\omega)\right]\mathbf{c}_{\text{st}}(\theta,\omega) \\ &\qquad + \overline{\mathbf{v}}_{\text{noise},i}(t) + \overline{\mathbf{v}}_{\text{jam},i}(t)\end{aligned}, \tag{29}$$

where

$$g_i(t,\theta,\theta_{\text{look}}) = \sum_{k=0}^{K} b_k(\theta,\theta_{\text{look}})\, a_{k,i}(t) \tag{30}$$

is, by linearity, the aggregation of the $K+1$ transmit beamformed responses to the ith pulse compression filter. The term in (30) could likewise be expressed as

$$g_i(t,\theta,\theta_{\text{look}}) = h_i(t) * \left[\sum_{k=0}^{K} b_k(\theta,\theta_{\text{look}})\, s_k(t)\right], \tag{31}$$

using $a_{k,i}(t) = h_i(t) * s_k(t)$, where the bracketed term in (31) is the far-field superposition of the $K+1$ emitted waveforms weighted by their respective beampatterns as a function of spatial angle.

Again assuming stationarity and statistical independence, the MIMO space-time covariance matrix for (29) is found to be

$$\begin{aligned}\mathbf{R}_i^{(\mathrm{MIMO})} &= E\left[\mathbf{z}_i(t)\ \mathbf{z}_i^H(t)\right] \\ &= \sum_{\omega}\sum_{\theta}\left[\left|g_i(t,\theta,\theta_{\mathrm{look}})\right|^2 * E\left|x(t,\theta,\omega)\right|^2\right]\mathbf{c}_{\mathrm{st}}(\theta,\omega)\ \mathbf{c}_{\mathrm{st}}^H(\theta,\omega) \\ &\quad + \bar{\mathbf{R}}_{\mathrm{noise}} + \bar{\mathbf{R}}_{\mathrm{jam}} \\ &= \sum_{\omega}\sum_{\theta}\left[\sigma_{\mathrm{clut}}^2(\theta,\omega)\int_{-T}^{T}\left|g_i(t,\theta,\theta_{\mathrm{look}})\right|^2 dt\right]\mathbf{c}_{\mathrm{st}}(\theta,\omega)\ \mathbf{c}_{\mathrm{st}}^H(\theta,\omega) \\ &\quad + \bar{\mathbf{R}}_{\mathrm{noise}} + \bar{\mathbf{R}}_{\mathrm{jam}}\end{aligned} \quad . \qquad (32)$$

Unlike the SIMO and SISO cases in (25) and (27), respectively, in which the transmit beamforming component is separable from the emitted waveform, the integral term in the MIMO covariance matrix of (32) is a non-separable function of the waveforms and their beampatterns that arise from the combination in (31). As such, greater design freedom exists that may be exploited to discriminate non-homogeneous clutter from moving targets. The degree to which there is utility in this trade-off of mainbeam power for greater sidelobe illumination for non-homogeneous interference cancellation remains to be seen, particularly given the system modifications necessary for MIMO compared to the rather minor modifications for the SIMO mode.

C) SIMO/MIMO μ-STAP SCM Analysis

Incorporating the SIMO, SISO, and MIMO analytical covariance matrices from (24), (27), and (32), respectively, into the associated primary and secondary SCM components from (18) and (19), along with the inclusion of non-homogeneous interference, reveals the true utility of the μ-STAP approach. Using (24), the expectation of the secondary SIMO SCM when non-homogeneous interference is present is thus

$$E\left[\hat{\mathbf{R}}_{\sec,i}^{(\mathrm{SIMO})}(\ell_{\mathrm{CUT}})\right] = \mathbf{R}_i^{(\mathrm{SIMO})} + \frac{1}{n(L_{\sec})}\sum_{\ell\in L_{\sec}}\sum_{\omega}\sum_{\theta}\left|b_0(\theta,\theta_{\mathrm{look}})\right|^2\left[\left(\sigma_{\mathrm{NH}}^2(t,\theta,\omega)*\left|a_{0,i}(t)\right|^2\right)\Big|_{t=\ell T_{\mathrm{samp}}}\right]\mathbf{c}_{\mathrm{st}}(\theta,\omega)\,\mathbf{c}_{\mathrm{st}}^H(\theta,\omega) \tag{33}$$

where $\sigma_{\mathrm{NH}}^2(t,\theta,\omega)$ is the power of the non-homogeneous scattering as a function of continuous time delay, angle, and Doppler, and T_{samp} is the sampling period. Likewise, again using the approximation of the primary filter response to the primary waveform as an impulse function [3], the expectation of the primary (SISO) SCM via (27) is

$$E\left[\hat{\mathbf{R}}_{\mathrm{prime}}^{(\mathrm{SIMO})}(\ell_{\mathrm{CUT}})\right] = \mathbf{R}^{(\mathrm{SISO})} + \frac{1}{n(L_{\mathrm{prime}})}\sum_{\substack{\ell\in L_{\mathrm{prime}}\\ \ell\neq\ell_{\mathrm{CUT}}}}\sum_{\omega}\sum_{\theta}\left|b_0(\theta,\theta_{\mathrm{look}})\right|^2\left[\left(\sigma_{\mathrm{NH}}^2(t,\theta,\omega)\right)\Big|_{t=\ell T_{\mathrm{samp}}}\right]\mathbf{c}_{\mathrm{st}}(\theta,\omega)\,\mathbf{c}_{\mathrm{st}}^H(\theta,\omega)\,. \tag{34}$$

The SISO SCM of (34) illustrates why contaminating targets in the training data can be problematic, since the $\sigma_{\mathrm{NH}}^2(t,\theta,\omega)$ term can lead to self-cancellation if corresponding to a target in the CUT with similar θ and ω. In contrast, the same target response in (33) is smeared over multiple range cells and is de-emphasized by the cross-correlation response $\left|a_{0,i}(t)\right|^2$. Further, while a clutter discrete in the CUT would be similarly smeared and de-emphasized in the secondary SCM of (33), the result is still an improvement over the primary SCM of (34) that excludes the clutter discrete altogether since the CUT snapshot is not included in the primary SCM.

Using (32), the expectation of the MIMO SCM for primary and secondary filtering is

$$E\left[\hat{\mathbf{R}}_i^{(\mathrm{MIMO})}(\ell_{\mathrm{CUT}})\right] = \mathbf{R}_i^{(\mathrm{MIMO})} + \frac{1}{n(L)}\sum_{\ell\in L}\sum_{\omega}\sum_{\theta}\left[\left(\sigma_{\mathrm{NH}}^2(t,\theta,\omega) * \left|g_i(t,\theta,\theta_{\mathrm{look}})\right|^2\right)\Big|_{t=\ell T_{\mathrm{samp}}}\right]\mathbf{c}_{\mathrm{st}}(\theta,\omega)\,\mathbf{c}_{\mathrm{st}}^H(\theta,\omega) \tag{35}$$

for $L = L_{\mathrm{sec}}$ when $i = 1, 2, \cdots, K$ and $L = L_{\mathrm{prime}}$ with $\ell \neq \ell_{\mathrm{CUT}}$ when $i = 0$. Clearly, the relationship between the secondary waveforms and beampatterns relative to the primary waveform and beampattern determines, via $\left|g_i(t,\theta,\theta_{\mathrm{look}})\right|^2$, how non-homogeneous interference in the CUT is represented in the SCM. In the following section it is demonstrated that a modest enhancement in SINR (even accounting for loss of primary mainbeam power) can be achieved under conditions of non-homogeneous interference for a simple MIMO emission scheme. The optimization of the secondary MIMO emissions (waveforms and associated beampatterns) and their associated receive filtering to maximize SINR (or perhaps some alternative metric) for GMTI in arbitrary non-homogeneous interference is left for later investigation. From a cognitive sensing perspective, it may also be possible to make these secondary emissions adaptive to the observed interference environment.

IV. SIMULATION RESULTS

Based on the model in [3], consider an airborne side-looking radar with no crab angle, $\beta = 1$, and look direction of $\theta_{\text{look}} = 0°$. The receive array is comprised of $N = 8$ uniform linear elements and the CPI consists of $M = 16$ pulses, so that $NM = 128$. The specific manner in which the secondary emissions are generated for the MIMO mode (i.e. implementation of sub-arrays/separate apertures with associated platform and mutual coupling effects) is not considered here. The signal/clutter model used here is relatively simple and serves the purpose of evaluating the impact of the various μ-STAP training data configurations to specific forms of interference non-homogeneity in a controlled manner. Separate work is investigating the prospective performance benefits on measured data.

The MIMO emission consists of a primary waveform and four secondary waveforms ($K = 4$) having time-bandwidth product $BT = 100$. The specific waveforms employed here are those whose response to the primary matched filter was shown in Fig. 1. The implementation and specific coding for the generation of these physical waveforms is taken from [36,37] and described in Appendix B. The SISO/SIMO emission is simply the primary beampattern in Fig. 2 while the secondary emission for the MIMO case consists of only the $k = 1$ secondary waveform using the omnidirectional beampattern illustrated in Fig. 2. It was previously shown in [1] that a spatial null could also be formed for the secondary beampattern in the direction of the primary mainbeam. It is expected that the need for additional secondary beams would only be warranted (given the additional loss to primary mainbeam power) if prior knowledge were available regarding known clutter effects (e.g. a collection of sidelobe discretes) relative to the mainbeam direction, for which another more focused secondary beam could be beneficial.

In [1] it was shown that the homogenization effect of this new secondary data provides enhanced detection and false alarm performance in non-homogeneous environments. Here the impact to SINR is evaluated. From [4] we shall use the SNR-normalized SINR metric

$$\frac{\text{SINR}}{\text{SNR}} = \frac{\sigma_v^2 \left|\mathbf{c}_{\text{st}}^H(\theta,\omega)\,\hat{\mathbf{R}}^{-1}\mathbf{c}_{\text{st}}(\theta,\omega)\right|^2}{(NM)\,\mathbf{c}_{\text{st}}^H(\theta,\omega)\hat{\mathbf{R}}^{-1}\mathbf{R}_{\text{o}}\hat{\mathbf{R}}^{-1}\mathbf{c}_{\text{st}}(\theta,\omega)}\left(\frac{P_{\text{prime}}}{P_{\text{total}}}\right), \tag{36}$$

where σ_v^2 is the noise power, $\mathbf{R}_{\text{o}}$ is the true clutter covariance for the CUT, and $\hat{\mathbf{R}}$ is the estimated SCM using some combination of training data (denoted in Table II). Relative to [4], the additional power ratio included in (36) represents the loss in the primary mainbeam for the MIMO emission ratio and is 1 for the SIMO/SISO case and is equal to 0.93 (–0.3 dB) for the secondary MIMO emission considered here. From (36) the (SNR-normalized) optimal SINR is

$$\frac{\text{SINR}_{\text{o}}}{\text{SNR}} = \frac{\sigma_v^2}{NM}\,\mathbf{c}_{\text{st}}^H(\theta,\omega)\,\mathbf{R}_{\text{o}}^{-1}\mathbf{c}_{\text{st}}(\theta,\omega)\left(\frac{P_{\text{prime}}}{P_{\text{total}}}\right), \tag{37}$$

which is obtained when $\hat{\mathbf{R}} = \mathbf{R}_{\text{o}}$. The ratio of (36) for either SIMO/SISO or MIMO to (37) for the SISO/SIMO condition provides the SINR_{o} normalized result

$$\frac{\text{SINR}}{\text{SINR}_{\text{o,SIMO}}} = \frac{\left|\mathbf{c}_{\text{st}}^H(\theta,\omega)\,\hat{\mathbf{R}}^{-1}\mathbf{c}_{\text{st}}(\theta,\omega)\right|^2}{\left(\mathbf{c}_{\text{st}}^H(\theta,\omega)\hat{\mathbf{R}}^{-1}\mathbf{R}_{\text{o}}\hat{\mathbf{R}}^{-1}\mathbf{c}_{\text{st}}(\theta,\omega)\right)\left(\mathbf{c}_{\text{st}}^H(\theta,\omega)\mathbf{R}_{\text{o}}^{-1}\mathbf{c}_{\text{st}}(\theta,\omega)\right)}\left(\frac{P_{\text{prime}}}{P_{\text{total}}}\right), \tag{38}$$

which we shall use to evaluate performance as a function of sample support that likewise accounts for the primary mainbeam power loss for the MIMO emission. Specifically, the value

$$\min_{\omega}\left[\frac{\mathrm{SINR}(\omega_{\mathrm{D}})}{\mathrm{SINR}_{\mathrm{o,SIMO}}(\omega_{\mathrm{D}})}\right] \tag{39}$$

is determined as the worst-case performance for each scenario as a function of the amount of training data according to the particular Doppler steering vectors of (6) and excluding the clutter notch. Here the clutter notch is conservatively defined to be the Doppler interval in which

$$\frac{\mathrm{SINR}_{\mathrm{o,SIMO}}(\omega_{\mathrm{D}})}{\mathrm{SNR}} < -0.5\ \mathrm{dB} \tag{40}$$

to avoid misrepresentative results at the edge of the notch. All the results considered are for the look direction $\theta = \theta_{\mathrm{look}}$.

From [3], we also consider the minimum detectable Doppler which is defined as

$$f_{\min} = \frac{1}{2}\left(f_{\mathrm{U}}(\mathrm{SINR}) - f_{\mathrm{L}}(\mathrm{SINR})\right) \tag{41}$$

where $f_{\mathrm{L}}(\mathrm{SINR})$ and $f_{\mathrm{U}}(\mathrm{SINR})$ demarcate the Doppler frequencies above and below the mainlobe clutter notch at which the designated value of SINR loss is attained. The minimum detectable velocity (MDV) can be directly obtained by multiplying this Doppler frequency by a half wavelength [3]. Thus the percent change in MDV, relative to that obtained for the standard SISO training data, can be determined as

$$\%\ \mathrm{MDV\ change} = \left(\frac{\mathrm{new}\ f_{\min} - \mathrm{SISO}\ f_{\min}}{\mathrm{SISO}\ f_{\min}}\right) \times 100\%\,. \tag{42}$$

To represent the continuous environment, the received signal descriptions of (2), (9), (10), and (20), along with the matched filters to be applied in (3) and (14), are "over-sampled" by a factor of 5 relative to the nominal 3-dB range resolution (the Nyquist criterion cannot be met for an ideal pulse that has theoretically infinite bandwidth). After the pulse compression stage of (3) or (14), each channel is decimated (lowpass filtered and downsampled) in range by 5 to obtain independent training data snapshots (from a primary data perspective).

From the five different channels of pulse compression filtered output via (14) there are multiple combinations of training data that could be used to obtain the SCM estimates of (1), (18), or (19) for both the SIMO and MIMO emission schemes. We shall show nine SINR performance curves, as indicated in Table II, for each interference scenario for both the SIMO and MIMO emission schemes. While these plots are rather busy, the point is to illustrate the impact of incorporating each additional channel of training data, with and without the inclusion of primary data. For each interference scenario tables are also provided to highlight selected performance comparisons in terms of SINR and MDV.

TABLE II. COMBINATIONS OF TRAINING DATA FOR SINR ANALYSIS

Training data used	**Line style/color**
primary	solid blue
primary, secondary k=1	solid green
primary, secondary k=1,2	solid red
primary, secondary k=1,2,3	solid teal
primary, secondary k=1,2,3,4	solid purple
secondary k=1	dashed green
secondary k=1,2	dashed red
secondary k=1,2,3	dashed teal
secondary k=1,2,3,4	dashed purple

Since the secondary snapshots do not provide independent data, the convergence is depicted in terms of the number of *range sample intervals*. For example, NM snapshots for the 'primary-only' case would translate to $5NM$ snapshots for the 'primary + 4 secondary' case, with both having the same (NM) range sample intervals. As such, even though the CUT snapshot need not be excised from the secondary training data, it is for these results so that a commensurate number of range sample intervals can be portrayed for each of the training data cases in Table II.

A) Homogeneous Clutter

The simulated noise is complex white Gaussian. The clutter is generated by dividing the range ring in azimuth into 136 equal-sized angle clutter patches, with the scattering from each patch being i.i.d. complex Gaussian. This spatial clutter distribution is weighted by the transmit beampattern and scaled such that, following coherent integration (pulse compression, beamforming, and Doppler processing) without clutter cancellation, the aggregate received clutter-to-noise ratio (CNR) is ~59 dB.

Figures 3-6 show the SNR-normalized (37) and worst-case SINR (39) results for the MIMO and SIMO emissions. Little difference is observed between the MIMO and SIMO cases for this scenario, with MIMO generally being at about a 0.2 dB disadvantage in the worst-case assessment, which arises from the power diverted from the primary mainbeam to enable the secondary emission. It is worth noting that convergence (as a function of sample intervals) increases rapidly as additional sources of training data are incorporated, though each successive new source of training data provides diminishing improvement. This result is to be expected since each filter response provides a different mixture (in range) of the same echo response surrounding the CUT demarcated by the extent of the auto/cross-correlations in range.

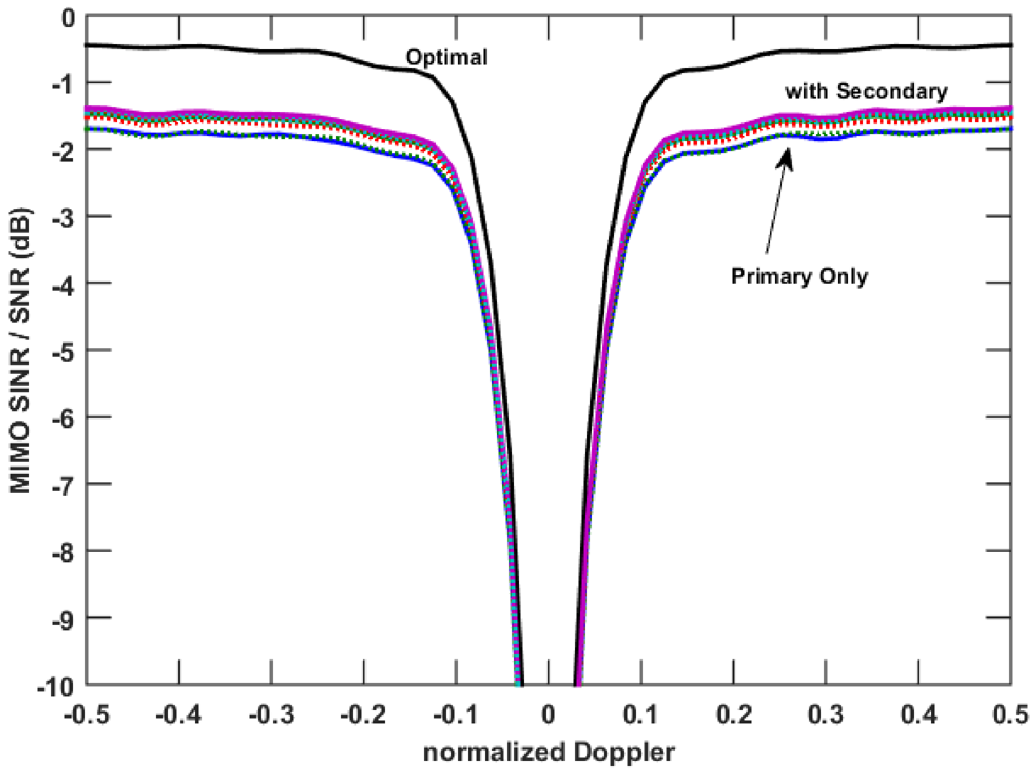

Fig. 3: SNR-normalized SINR for homogeneous clutter (MIMO)

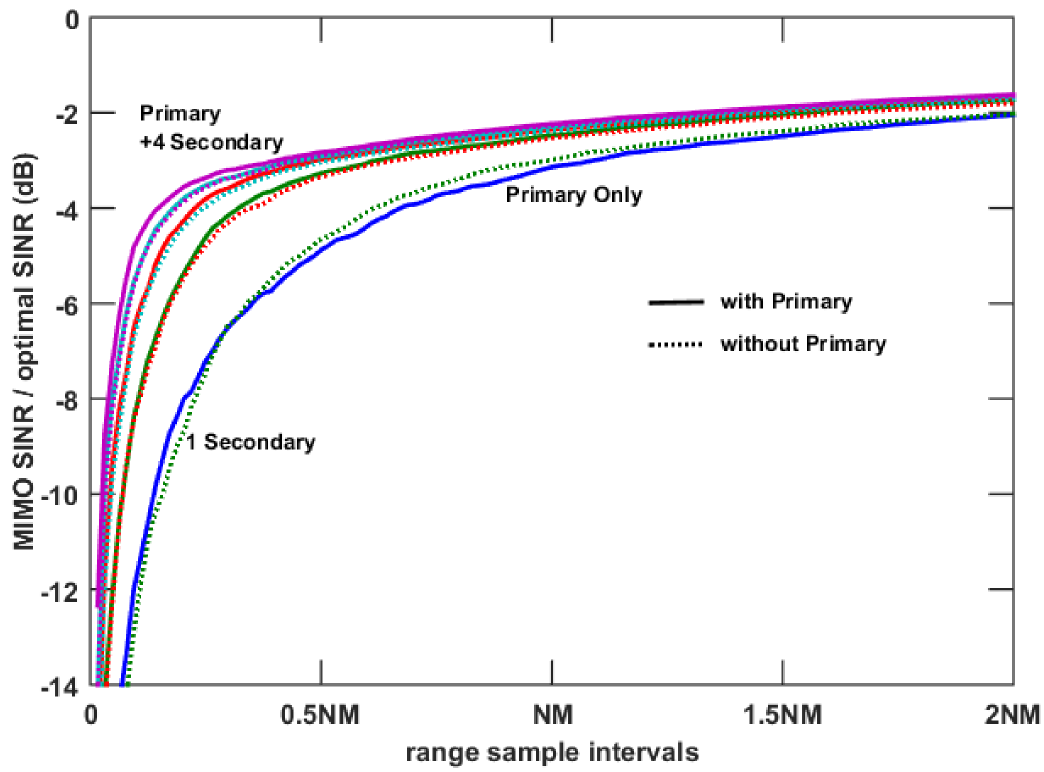

Fig. 4: Worst-case $SINR_o$-normalized SINR for homogeneous clutter (MIMO)

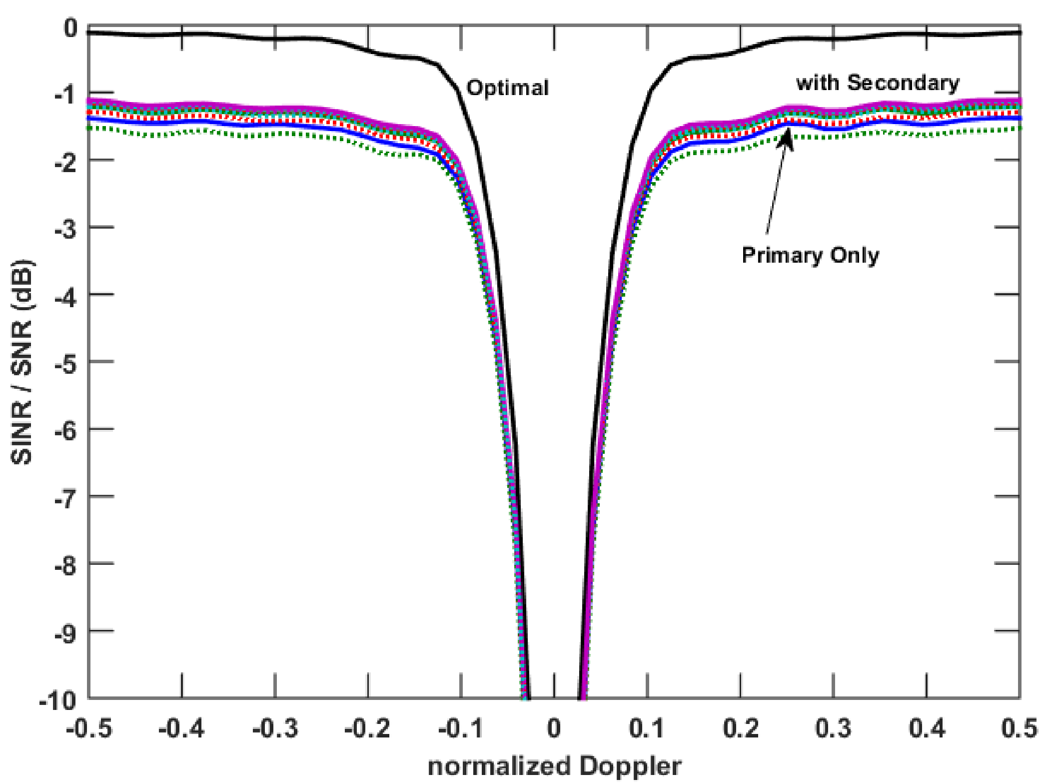

Fig. 5: SNR-normalized SINR for homogeneous clutter (SIMO)

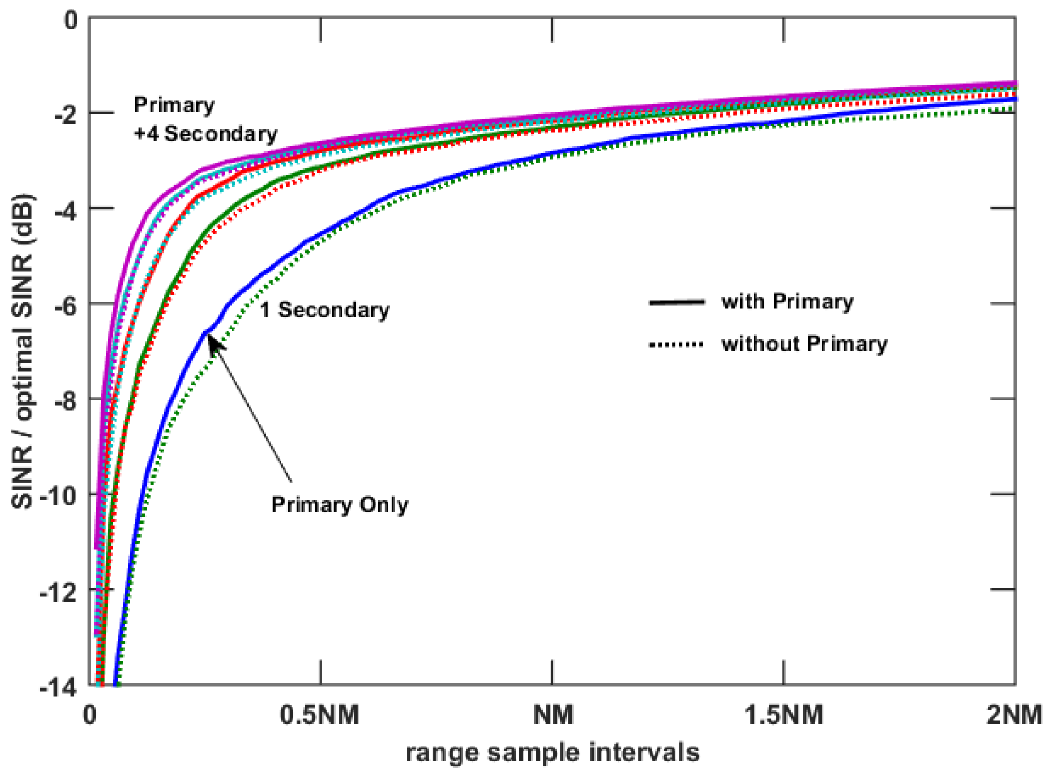

Fig. 6: Worst-case $SINR_o$-normalized SINR for homogeneous clutter (SIMO)

Per Table III, the case involving the MIMO emission using only the primary training data generally performs the worst (highlighted in red), though it is only marginally worse than standard SISO (i.e. SIMO primary only). The best MIMO configuration employs the 'primary + 4 secondary' training data sets, achieving performance improvements relative to standard SISO of 1.7 dB, 0.6 dB, and 0.1 dB, respectively, for 0.5*NM*, *NM*, and 2*NM* range sample intervals. The best SIMO configuration is likewise the 'primary + 4 secondary' training data sets with performance improvements relative to standard SISO of 1.9 dB, 0.8 dB, and 0.3 dB for 0.5*NM*, *NM*, and 2*NM* range sample intervals, respectively. The latter is also the best performing of those considered. It is interesting to note that both the SIMO and MIMO 'k = 1 secondary' cases (dashed green) yield SINR responses nearly identical to that of standard SISO.

TABLE III. CONVERGENCE COMPARISON FOR HOMOGENEOUS CLUTTER (RED: WORST, GREEN: BEST MIMO, BLUE: BEST SIMO)

Emission, training	**0.5NM**	**NM**	**2NM**
MIMO, prime	–4.9 dB	–3.1 dB	–2.0 dB
MIMO, prime + 1 sec.	–3.3 dB	–2.5 dB	–1.7 dB
MIMO, prime + 4 sec.	–2.8 dB	–2.2 dB	–1.6 dB
MIMO, 1 sec.	–4.7 dB	–3.0 dB	–2.0 dB
MIMO, 4 sec.	–2.9 dB	–2.3 dB	–1.6 dB
SIMO, prime (SISO)	–4.5 dB	–2.8 dB	–1.7 dB
SIMO, prime + 1 sec.	–3.1 dB	–2.3 dB	–1.5 dB
SIMO, prime + 4 sec.	–2.6 dB	–2.0 dB	–1.4 dB
SIMO, 1 sec.	–4.7 dB	–2.9 dB	–1.9 dB
SIMO, 4 sec.	–2.7 dB	–2.1 dB	–1.4 dB

The reason that the μ-STAP implementations using 2 or more sets of training data outperform the standard ‘primary only’ SISO case (solid blue) for this homogeneous clutter scenario is because the additional training data provides different mixtures of an extended segment of clutter samples due to the range-extended smearing (see Fig. 1). Given BT = 100 for all these waveforms and one sample per range cell (after down-sampling as discussed before), the secondary responses capture nearly $2BT$ more clutter samples than the range-focused primary response. Accounting for this increased sample support for the SISO case (i.e. using $2NM + 2BT$ snapshots) would yield a value of $\mathrm{SINR/SINR_o} = -1.1\ \mathrm{dB}$, which upper bounds all of the μ-STAP implementations (and likewise for all the results to follow). If the nature of the clutter were to change significantly as a function of range (e.g. in a littoral environment) such that one would wish to avoid this range extension effect, then the problem becomes one of properly designing the secondary filters according to the resulting cross-correlation responses and then judiciously selecting the secondary training data that is produced.

It is also interesting to consider the impact of these different sets of training data upon the minimum detectable velocity (MDV). Table IV provides comparisons of the minimum detectable Doppler f_{min} from (41) for two different normalized SINR values, as well as the resulting percent change in MDV via (42). For the MIMO emission using only the primary training data, modest degradation in MDV is observed (note that the f_{min} values are already small). Using all four sets of secondary training data for the MIMO case then yields essentially the same performance as standard SISO. The SIMO case using 'primary + 4 secondary' training data sets does provide a minor MDV improvement, though again relative to already small f_{min} values.

TABLE IV. MDV COMPARISON FOR HOMOGENEOUS CLUTTER AT 2NM SAMPLE INTERVALS (RED: WORST, GREEN: BEST)

@ –3 dB SINR/SNR	normalized f_{min}	% MDV change
SIMO, prime **(SISO)**	0.0855	0.0%
SIMO, prime + 4 sec.	0.0810	–5.3%
MIMO, prime	0.0935	+9.4%
MIMO, prime + 4 sec.	0.0855	0.0%
@ –10 dB SINR/SNR	normalized f_{min}	% change from SISO
SIMO, prime **(SISO)**	0.0325	0.0%
SIMO, prime + 4 sec.	0.0320	–1.5%
MIMO, prime	0.0340	+4.6%
MIMO, prime + 4 sec.	0.0330	+1.5%

B) Non-Homogeneous Clutter

To model non-homogeneous clutter [3], the power of the complex Gaussian homogeneous clutter patches is randomly modulated for each range/angle clutter patch based on a Weibull distribution with a shape parameter of 1.7 [47,48]. In addition to this 'local' modulation, a 'regional' modulation is also imposed using an exponential distribution with $\lambda = 0.05$ and applied independently to each region, which comprises an area of clutter patches corresponding to 10 range cells ("over-sampled" by 5 as discussed above) × $1/N$ angle segments (of the 136 in each range ring). The clutter in the particular range swath that includes the CUT is increased by an additional 10 dB to ensure sufficient clutter power in the CUT after random assignment. The overall clutter response is normalized to maintain a consistent average clutter power. Internal clutter motion is also incorporated that is uniformly distributed on ±0.02 normalized Doppler for each clutter patch. This model is not necessarily a representation of a particular measured instantiation of non-homogeneous clutter but is used to indicate the STAP responses under significant variability in range, angle, and Doppler.

Figures 7-10 illustrate the SNR-normalized SINR (37) and the worst-case SINR (39) for the MIMO/SIMO emissions and the different sets of training data. As a function of Doppler, Figs. 7 and 9 show the expected wider clutter notch, as compared to the homogeneous clutter case from Figs. 3 and 5, which results from internal clutter motion. Overall, slower convergence is observed for the non-homogeneous clutter case compared to homogeneous clutter, particularly for the 'primary only' training data, though the use of secondary data reduces the gap. As expected [5], much more training data is required for non-homogeneous clutter to attain the same SINR performance as the homogeneous clutter case.

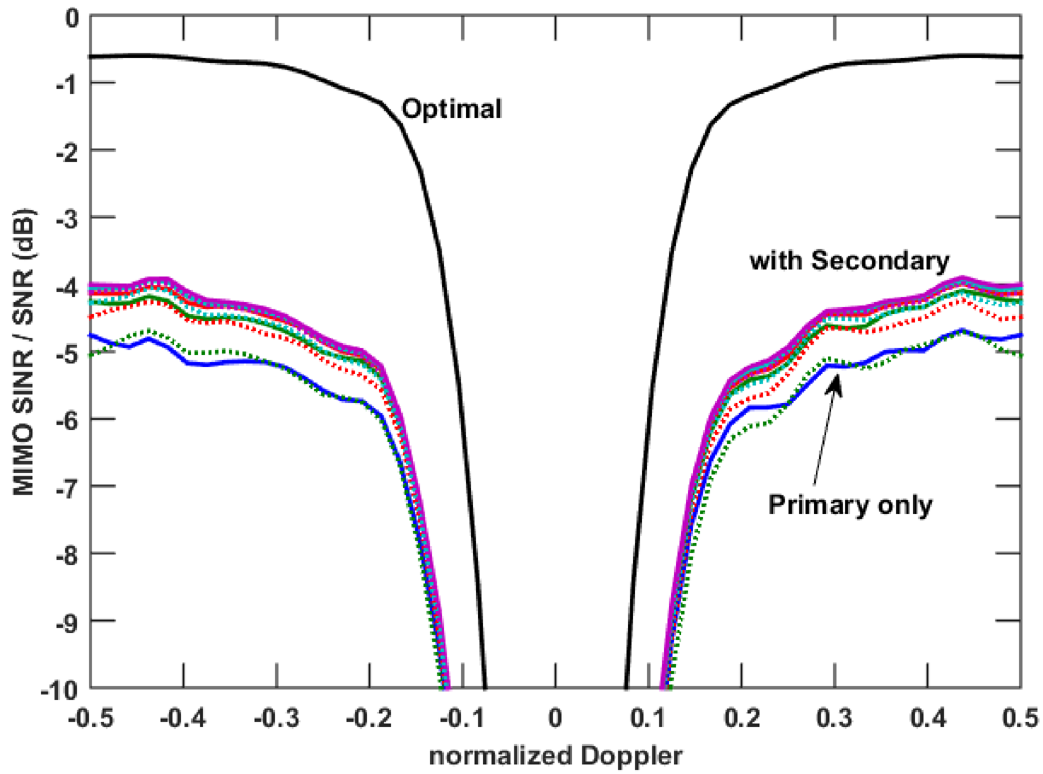

Fig. 7: SNR-normalized SINR for non-homogeneous clutter (MIMO)

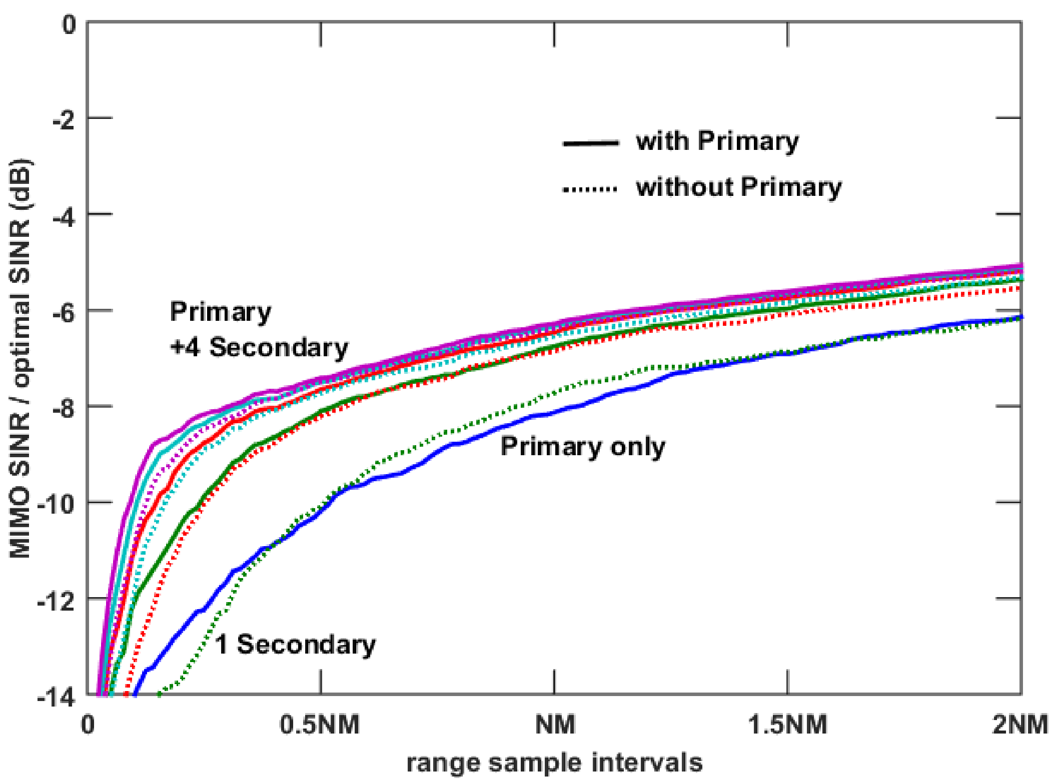

Fig. 8: Worst-case $SINR_o$-normalized SINR for non-homogeneous clutter (MIMO)

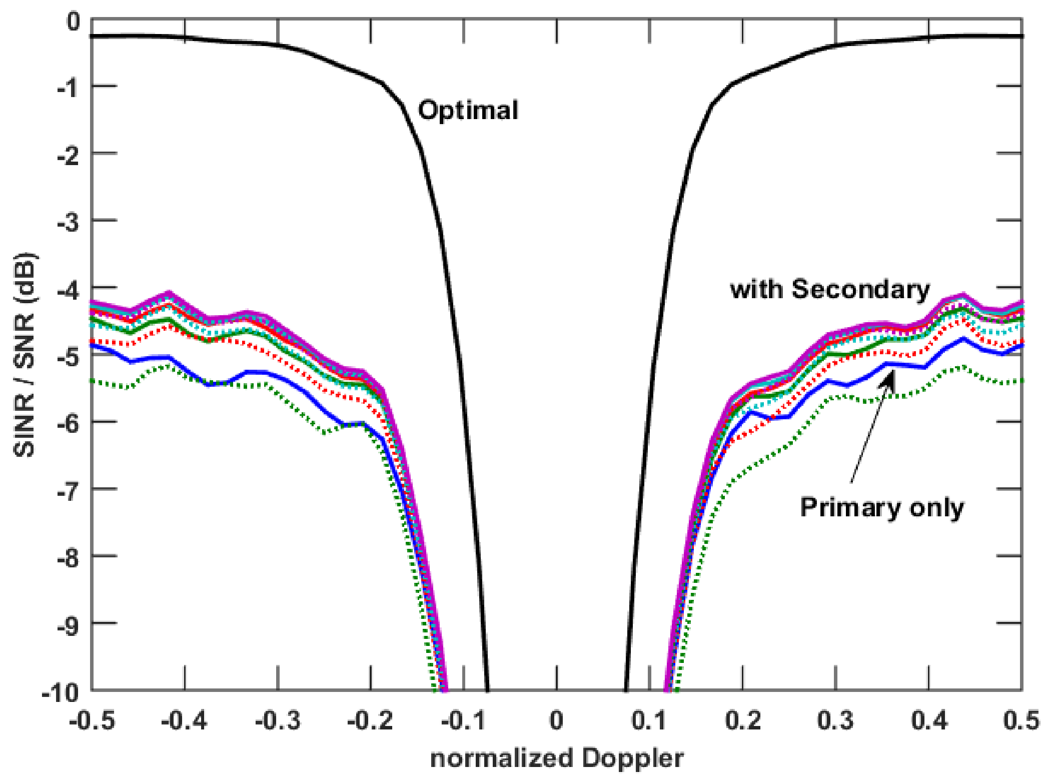

Fig. 9: SNR-normalized SINR for non-homogeneous clutter (SIMO)

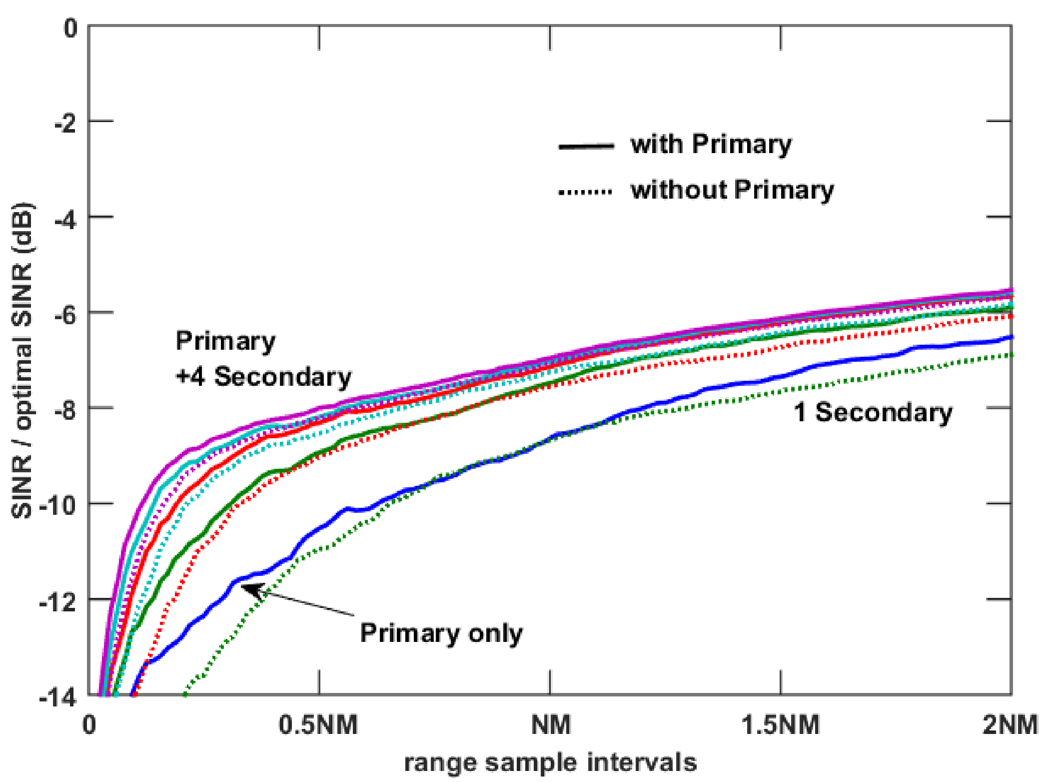

Fig. 10: Worst-case $SINR_o$-normalized SINR for non-homogeneous clutter (SIMO)

Per Table V, the MIMO emission now provides an enhancement over SIMO for all training data sets, with the ‘primary + 4 secondary’ MIMO case providing 3.1 dB, 2.3 dB, and 1.4 dB improvement over ‘primary only’ SIMO (standard SISO) at 0.5*NM*, *NM*, and 2*NM* range sample intervals, respectively. The ‘primary + 4 secondary’ SIMO case comes in a close second with 2.5 dB, 1.6 dB, and 1.0 dB improvement over ‘primary only’ SIMO (standard SISO) at the same range sample intervals. In Table VI an MDV enhancement is also observed for each of the implementations relative to standard SISO. The most significant improvement is obtained with the MIMO ‘primary +4 secondary’ case, while the SIMO ‘primary +4 secondary’ case is again in second place.

TABLE V. CONVERGENCE COMPARISON FOR NON-HOMOGENEOUS CLUTTER (RED: WORST, GREEN: BEST MIMO, BLUE: BEST SIMO)

Emission, training	**0.5NM**	**NM**	**2NM**
MIMO, prime	–10.2 dB	–8.1 dB	–6.1 dB
MIMO, prime + 1 sec.	–8.1 dB	–6.8 dB	–5.4 dB
MIMO, prime + 4 sec.	–7.4 dB	–6.3 dB	–5.1 dB
MIMO, 1 sec.	–10.1 dB	–7.7 dB	–6.2 dB
MIMO, 4 sec.	–7.5 dB	–6.4 dB	–5.2 dB
SIMO, prime **(SISO)**	–10.5 dB	–8.6 dB	–6.5 dB
SIMO, prime + 1 sec.	–8.9 dB	–7.5 dB	–5.9 dB
SIMO, prime + 4 sec.	–8.0 dB	–7.0 dB	–5.5 dB
SIMO, 1 sec.	–11.0 dB	–8.7 dB	–6.9 dB
SIMO, 4 sec.	–8.2 dB	–7.1 dB	–5.7 dB

TABLE VI. MDV COMPARISON FOR NON-HOMOGENEOUS CLUTTER AT 2NM SAMPLE INTERVALS (RED: WORST, GREEN: BEST)

@ –7 dB SINR/SNR	normalized f_{min}	% change from SISO
SIMO, prime **(SISO)**	0.1655	0.0%
SIMO, prime + 4 sec.	0.1550	–6.3%
MIMO, prime	0.1595	–3.6%
MIMO, prime + 4 sec.	0.1475	–10.9%
@ –10 dB SINR/SNR	normalized f_{min}	% change from SISO
SIMO, prime **(SISO)**	0.1220	0.0%
SIMO, prime + 4 sec.	0.1185	–2.9%
MIMO, prime	0.1195	–2.0%
MIMO, prime + 4 sec.	0.1145	–6.1%

C) Clutter Discrete in CUT

Another form of non-homogeneous interference occurs when a clutter discrete resides in the CUT (with no similar responses in surrounding training data) [6]. Here, we consider the case of such a discrete that is 20 dB above the average response of the other clutter patches and arrives in the mainbeam direction. The remainder of the clutter is otherwise non-homogeneous as described in the previous section. Thus, the interference in the CUT is different from that in the surrounding primary (SISO) training data, thereby resulting in uncancelled clutter. Figures 11-14 show the SNR-normalized SINR and worst-case SINR for the MIMO/SIMO emissions for non-homogeneous clutter with a clutter discrete in the CUT. The results are qualitatively the same as Figs. 7-9, albeit with a further SINR degradation of 1 to 4 dB depending on the training data being used.

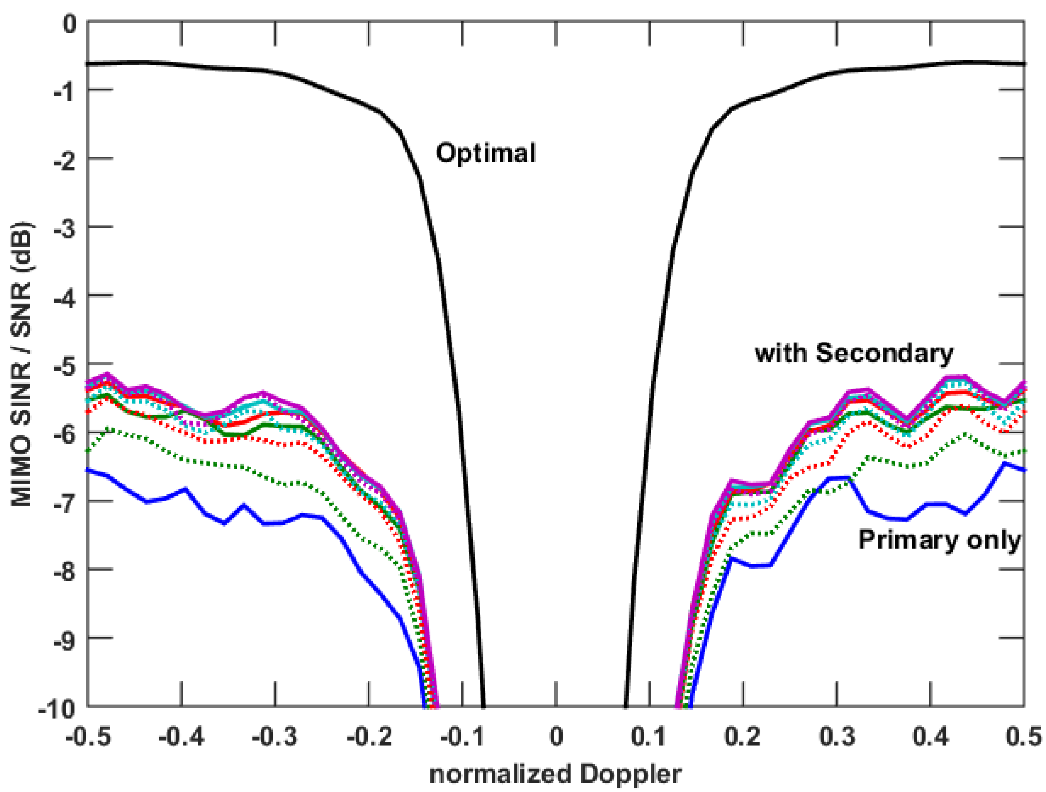

Fig. 11: SNR-normalized SINR for large clutter discrete in CUT (MIMO)

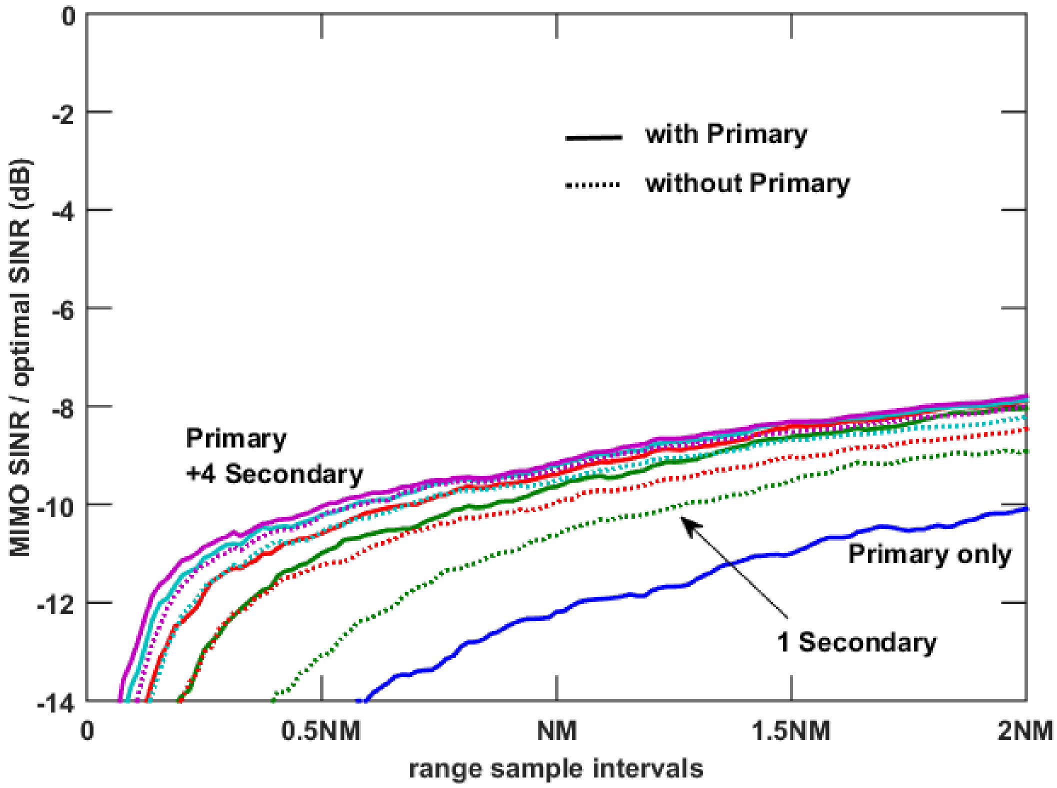

Fig. 12: Worst-case $SINR_o$-normalized SINR for large clutter discrete in CUT (MIMO)

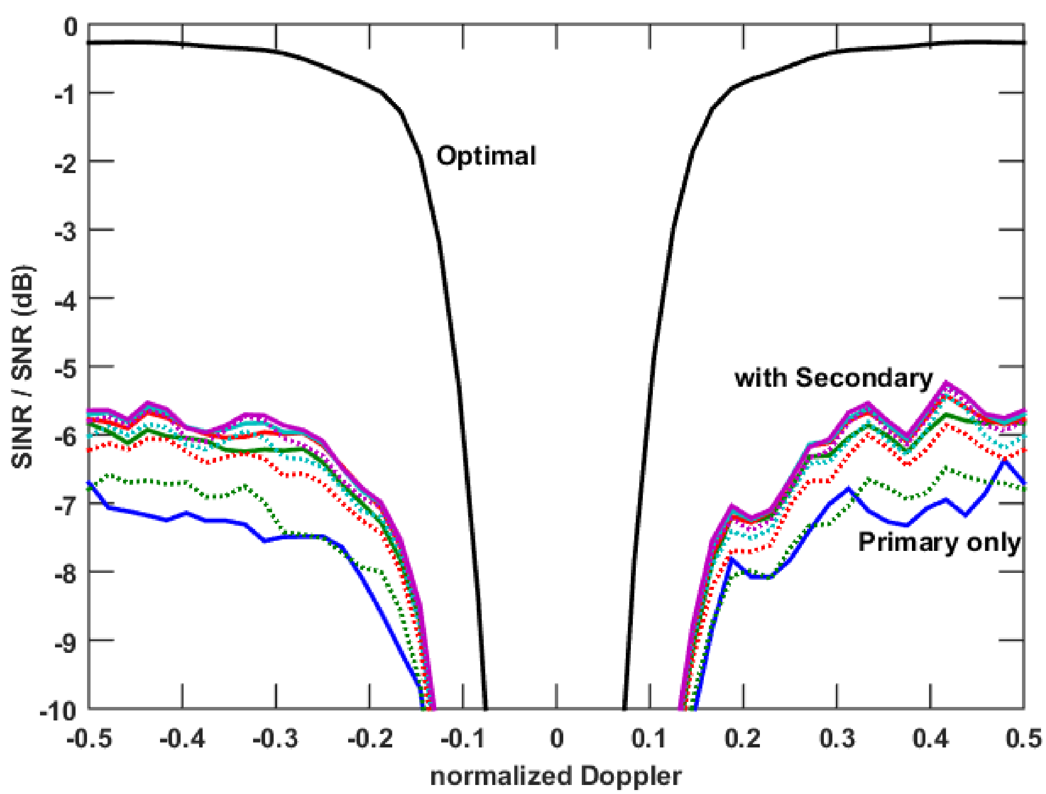

Fig. 13: SNR-normalized SINR for large clutter discrete in CUT (SIMO)

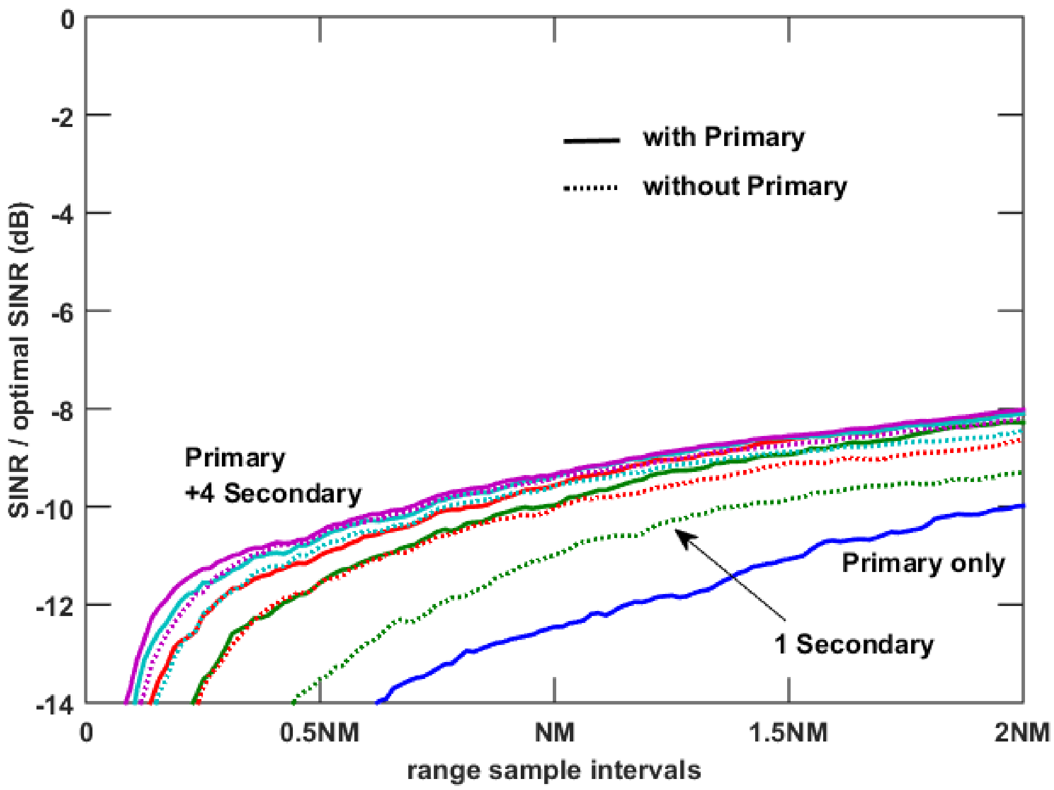

Fig. 14: Worst-case $SINR_o$-normalized SINR for large clutter discrete in CUT (SIMO)

From Table VII, the ‘primary + 4 secondary’ data for both MIMO and SIMO cases demonstrate enhanced performance relative to SISO. The former yielding an improvement of 4.6 dB, 3.3 dB, and 2.2 dB and the latter 4.1 dB, 3.2 dB, and 2.0 dB improvement at 0.5*NM*, *NM*, and 2*NM* range sample intervals, respectively. Likewise, in Table VIII it is shown that both of these training data sets provide a marked reduction in MDV, which is really due to less MDV degradation for these cases relative to the previous scenario when the clutter discrete was absent.

TABLE VII. CONVERGENCE COMPARISON FOR NON-HOMOGENEOUS CLUTTER + CLUTTER DISCRETE (RED: WORST, GREEN: BEST MIMO, BLUE: BEST SIMO)

Emission, training	**0.5NM**	**NM**	**2NM**
MIMO, prime	–14.3 dB	–12.2 dB	–10.1 dB
MIMO, prime + 1 sec.	–11.0 dB	–9.6 dB	–8.0 dB
MIMO, prime + 4 sec.	–10.0 dB	–9.2 dB	–7.8 dB
MIMO, 1 sec.	–13.1 dB	–10.6 dB	–8.9 dB
MIMO, 4 sec.	–10.2 dB	–9.3 dB	–8.0 dB
SIMO, prime (SISO)	–14.6 dB	–12.5 dB	–10.0 dB
SIMO, prime + 1 sec.	–11.6 dB	–10.0 dB	–8.3 dB
SIMO, prime + 4 sec.	–10.5 dB	–9.3 dB	–8.0 dB
SIMO, 1 sec.	–13.5 dB	–11.0 dB	–9.3 dB
SIMO, 4 sec.	–10.6 dB	–9.4 dB	–8.2 dB

TABLE VIII. MDV COMPARISON FOR NON-HOMOGENEOUS CLUTTER + CLUTTER DISCRETE AT 2NM SAMPLE INTERVALS (RED: WORST, GREEN: BEST)

@ –8 dB SINR/SNR	normalized $f_{\min}$	% change from SISO
SIMO, prime (SISO)	0.1980	0.0%
SIMO, prime + 4 sec.	0.1580	–20.2%
MIMO, prime	0.1965	–0.8%
MIMO, prime + 4 sec.	0.1515	–23.5%
@ –10 dB SINR/SNR	normalized $f_{\min}$	% change from SISO
SIMO, prime (SISO)	0.1455	0.0%
SIMO, prime + 4 sec.	0.1315	–9.6%
MIMO, prime	0.1420	–2.4%
MIMO, prime + 4 sec.	0.1280	–12.0%

D) 10 Targets in Training Data

The final case considers the impact of 10 targets of 15 dB SNR (and random independent phase responses) in the training data with normalized Doppler of 0.5. These targets reside in the first 10 training data samples and, being of modest SNR within non-homogeneous clutter as described earlier, may not be easily found by non-homogeneity detection. The purpose of this evaluation is to ascertain the degree of self-cancellation that occurs for the various SIMO and MIMO μ-STAP training data formulations since the cross-correlation “smearing” would ensure these target responses are incorporated into all the surrounding secondary training data samples.

Whereas the previous case involving a CUT clutter discrete realized degradation across all Doppler, Figs. 15-18 show that all the different combinations of training data exhibit an SINR loss at the associated targets’ Doppler. The SCMs based on secondary data still outperform the standard SISO case formed only from primary data. Further, unlike the previous three scenarios, both MIMO and SIMO results for this case reveal that the exclusion of primary data from the SCM (previously referred to as the ‘no primary’ μ-STAP configurations of (19)) is preferable from an SINR standpoint due to contamination of the training data (which is lessened in the smeared secondary data).

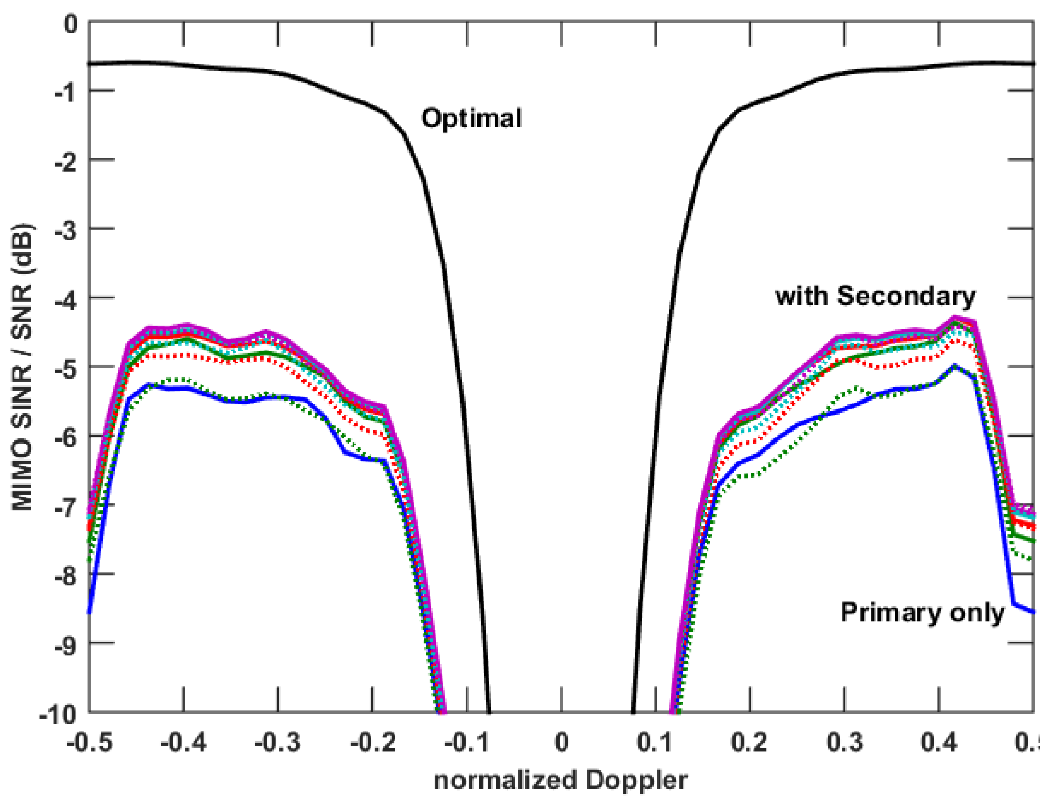

Fig. 15: SNR-normalized SINR for large target in training data (MIMO)

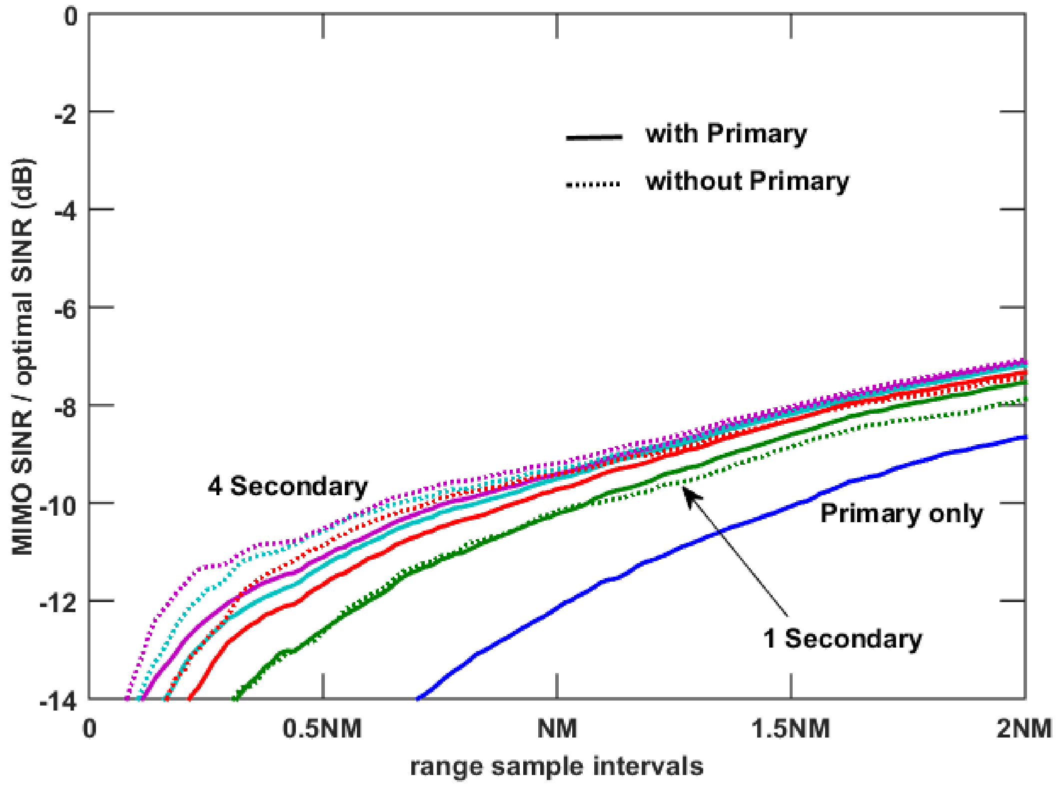

Fig. 16: Worst-case SINR$_o$-normalized SINR for large target in training data (MIMO)

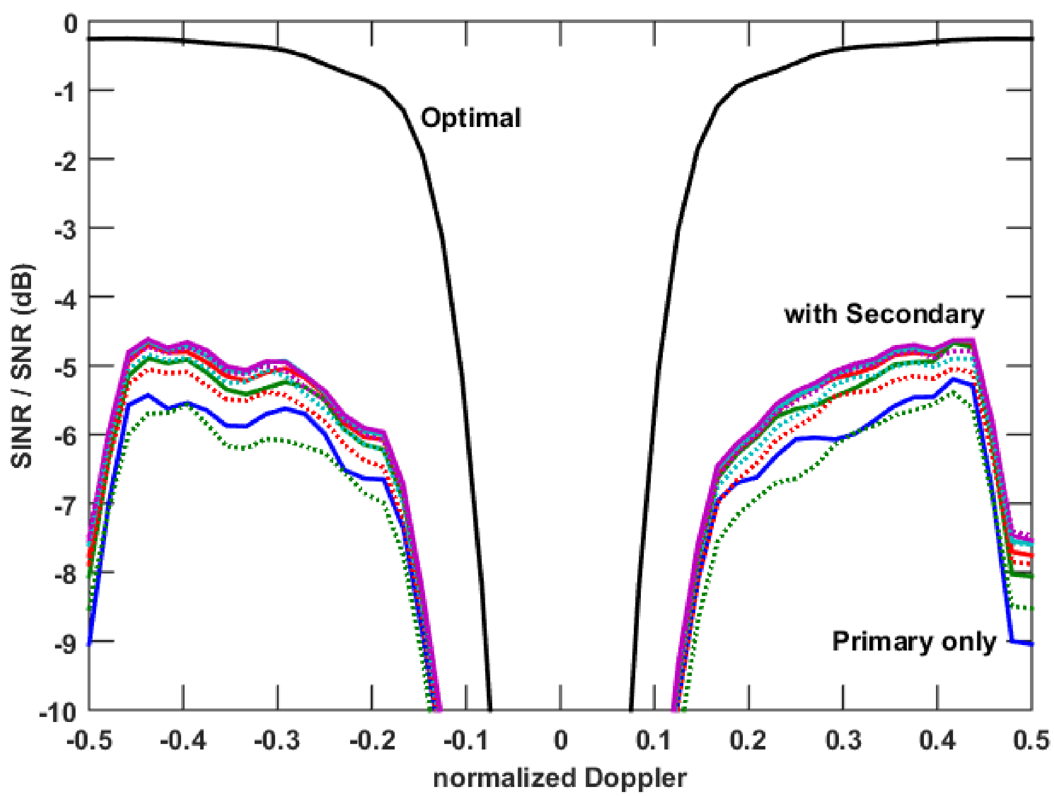

Fig. 17: SNR-normalized SINR for large target in training data (SIMO)

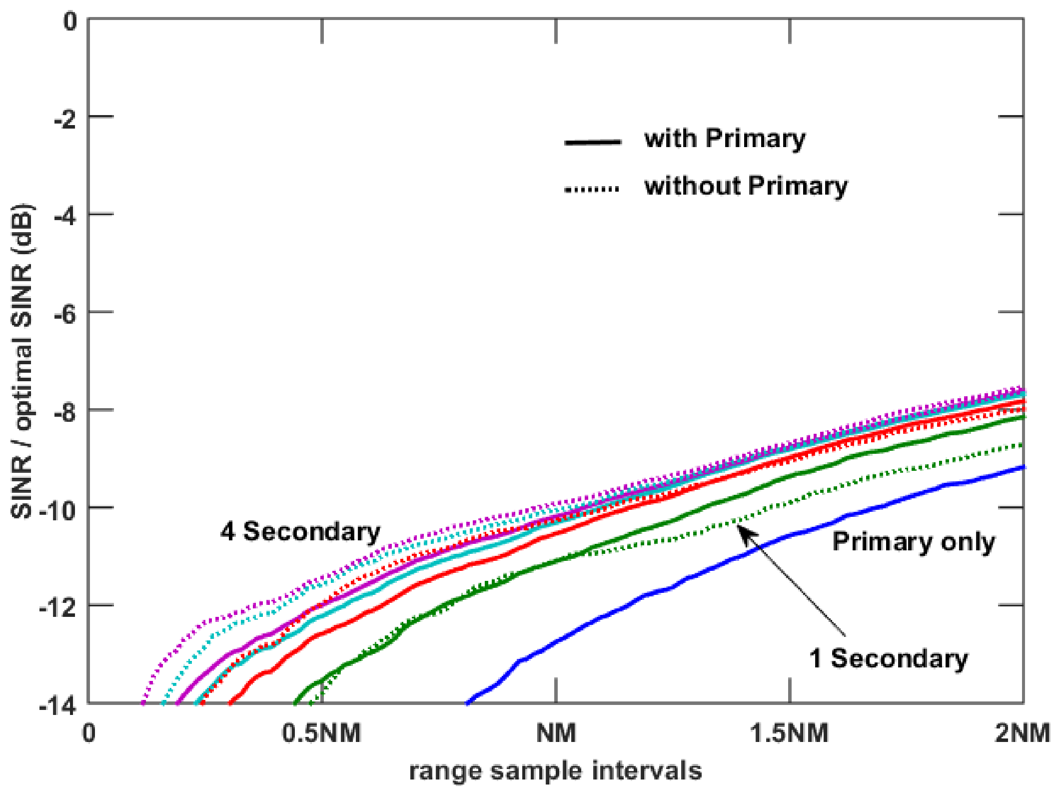

Fig. 18: Worst-case $SINR_o$-normalized SINR for large target in training data (SIMO)

Now the MIMO emission using ‘4 secondary (no primary)’ filters provides the best performance with an improvement of 6.0 dB, 3.5 dB, and 2.1 dB over the ‘primary only’ SIMO case (standard SISO) at 0.5*NM*, *NM*, and 2*NM* range sample intervals, respectively, according to Table IX. The MIMO ‘primary + 4 secondary’ case is the next best, followed close behind by the SIMO ‘4 secondary (no primary)’ case. The MDV results for this scenario shown in Table X are quite similar to those observed for non-homogeneous clutter, with the different μ-STAP training data sets providing an improvement relative to the SISO training data.

TABLE IX. CONVERGENCE COMPARISON NON-HOMOGENEOUS CLUTTER + 10 TRAINING DATA TARGETS (RED: WORST, GREEN: BEST MIMO, BLUE: BEST SIMO)

Emission, training	**0.5NM**	**NM**	**2NM**
MIMO, prime	–15.9 dB	–12.1 dB	–8.7 dB
MIMO, prime + 1 sec.	–12.6 dB	–10.2 dB	–7.5 dB
MIMO, prime + 4 sec.	–11.1 dB	–9.4 dB	–7.1 dB
MIMO, 1 sec.	–12.6 dB	–10.2 dB	–7.9 dB
MIMO, 4 sec.	–10.5 dB	–9.2 dB	–7.1 dB
SIMO, prime (SISO)	–16.5 dB	–12.7 dB	–9.2 dB
SIMO, prime + 1 sec.	–13.6 dB	–11.1 dB	–8.1 dB
SIMO, prime + 4 sec.	–12.0 dB	–10.2 dB	–7.6 dB
SIMO, 1 sec.	–13.8 dB	–11.1 dB	–8.7 dB
SIMO, 4 sec.	–11.4 dB	–9.9 dB	–7.5 dB

TABLE X. MDV COMPARISON FOR NON-HOMOGENEOUS CLUTTER + 10 TRAINING DATA TARGETS AT 2NM SAMPLE INTERVALS (RED: WORST, GREEN: BEST)

@ –7 dB SINR/SNR	normalized $f_{\min}$	% change from SISO
SIMO, prime (SISO)	0.1715	0.0%
SIMO, prime + 4 sec.	0.1600	–6.7%
MIMO, prime	0.1650	–3.8%
MIMO, prime + 4 sec.	0.1530	–10.8%
@ –10 dB SINR/SNR	normalized $f_{\min}$	% change from SISO
SIMO, prime (SISO)	0.1285	0.0%
SIMO, prime + 4 sec.	0.1235	–3.9%
MIMO, prime	0.1250	–2.7%
MIMO, prime + 4 sec.	0.1205	–6.2%

It is worth noting, since the secondary filters produce a smearing in range, that the case in which the target is in the CUT can exhibit some SINR degradation for the various μ-STAP implementations relative to standard SISO STAP (for which the CUT snapshot is excluded from the SCM). For the STAP parameterization considered here with homogeneous clutter and the given set of secondary filters, it has been found that if the target SNR exceeds about 22 dB then the SISO case and the SIMO cases that include the primary data yield effectively the same worst-case SINR performance (via (39)) when 2NM range sample intervals of training data are used for SCM estimation (with commensurate performance for the MIMO instantiation). If the CUT target SNR is higher still, then the addition of further secondary training data channels in the SCM induces further SINR losses to a modest degree.

For example, if the target in the CUT has a 30 dB SNR, then up to 1.8 dB of SINR degradation occurs when all four secondary filters are used, though this amount of loss on a 30 dB target response is not all that significant. However, this example highlights the difference one would obtain from using μ-STAP training data relative to the standard primary training data. Of course, when targets in the training data have sufficient SNR, non-homogeneity detection can be employed to excise/de-emphasize the associated training data snapshots. Such an approach may likewise be employed for the new form of secondary training data described here through some variant of the CLEAN algorithm [49].

CONCLUSIONS

A multi-waveform variant of STAP, denoted as μ-STAP, has been proposed that provides additional training data obtained from secondary pulse compression filters that may or may not actually correspond to waveforms that have been transmitted. In a MIMO instantiation, low-power secondary waveforms having low cross-correlation with the primary (traditional GMTI) waveform are emitted, with the stipulation that the secondary beampatterns have low gain in the direction of the primary mainbeam. This requirement serves to maximize the separability of the clutter generated by the primary and secondary emissions, thus enhancing suppression of non-homogeneous interference in the spatial sidelobes while maintaining sufficient cancellation of mainlobe clutter for target detection.

Alternatively, a SIMO instantiation is also proposed in which only the primary waveform is emitted yet the secondary filters are still applied to the received signal. This SIMO mode thus requires no hardware/antenna modification to the radar system. In both the MIMO and SIMO cases the additional training data from the secondary filters provides a range-smeared response for the mainbeam clutter that serves to improve robustness to non-homogeneous clutter, clutter discretes, and targets in the training data. Ongoing work is exploring how existing robust STAP implementations could incorporate these secondary training data sets.

APPENDIX A: MONTE CARLO OF WAVEFORM CROSS-CORRELATIONS

We evaluate the integral $\int_{-T}^{T} \left| a_{0,i}(t) \right|^2 dt$ from (25) for arbitrary FM waveforms by leveraging the PCFM implementation from [36,37] in which an arbitrary polyphase code is used to define a constant modulus, continuous, and spectrally well-contained FM waveform amenable for high-power emissions. As such, characterization of the cross-correlation response using such waveforms provides an accurate representation of possible performance for practical waveforms.

For each Monte Carlo trial, two waveforms are generated from independent length N_{code} sequences of *phase-change* parameters α randomly drawn according to a uniform distribution in the interval $[-\pi, \pi]$, where N_{code} closely approximates the time-bandwidth product [36]. Here, time-bandwidth products (*BT*) of 20, 50, 100, 150, and 200 are considered. For each trial, the normalized cross-correlation (by *BT* and the "over-sampling" factor relative to 3 dB bandwidth) is evaluated in terms of integrated cross-correlation sidelobe response $\int_{-T}^{T} \left| a_{0,i}(t) \right|^2 dt$ such as appears in (25) and (33). A Monte Carlo aggregated peak cross-correlation sidelobe response from (16) is also shown to provide insight into waveform separability as a function of *BT*.

Figure 19 illustrates the results of the Monte Carlo trials for integrated cross-correlation, which is observed to become more tightly bound to unity as *BT* increases, thus ensuring that secondary training data provides an estimate of the covariance matrix commensurate with that of the primary training data. Figure 20 also shows the peak cross-correlation sidelobe responses for the different *BT* values. As expected, the trend shows the peak response decreasing in general with increasing *BT*. Note that these waveforms were randomly generated so that a lower peak response would be expected if actual optimization of the metric in (16) were performed.

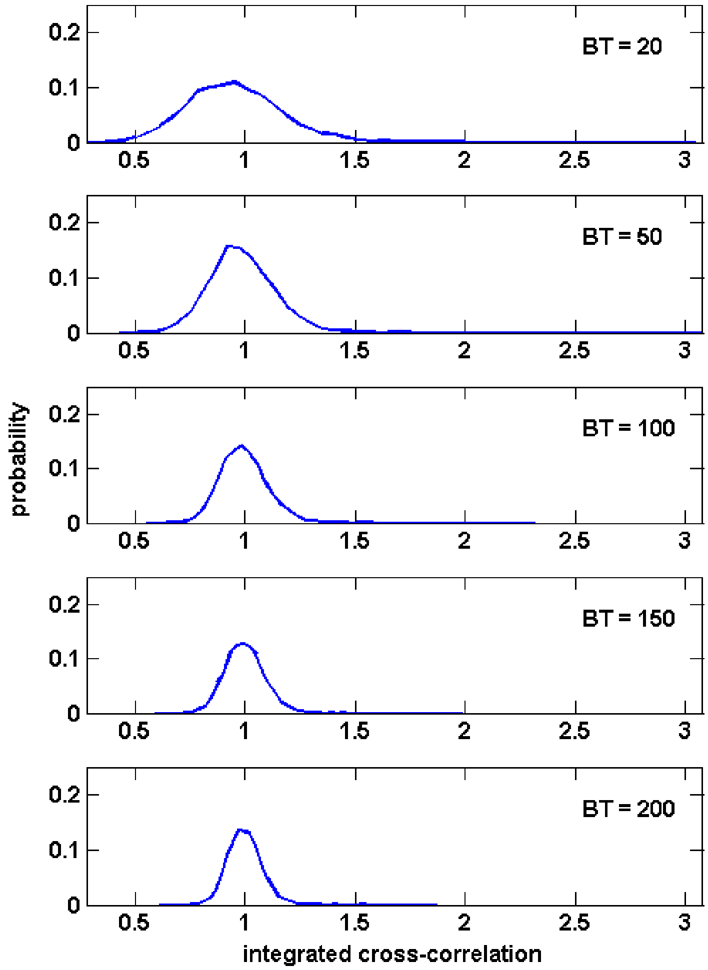

Fig. 19: Integrated cross-correlation response – Monte Carlo results

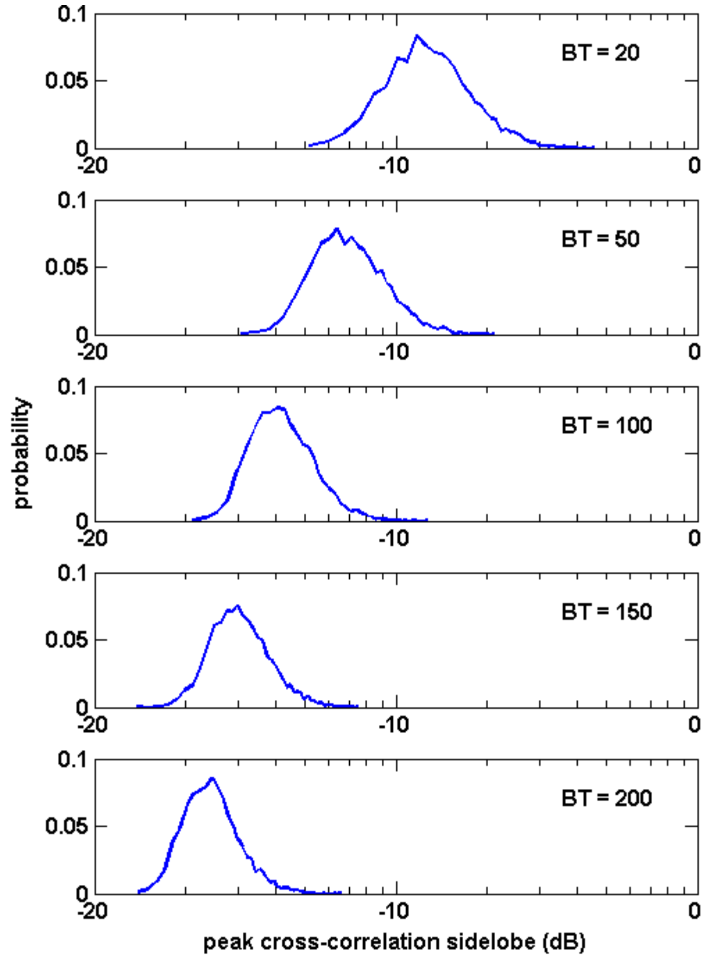

Fig. 20: Peak cross-correlation response – Monte Carlo results

Appendix B: Implementation of Physical Waveforms

The $K+1=5$ waveforms with BT = 100 used in the simulation results are based on the PCFM implementation described in [36,37] that enables the generation of arbitrary FM waveforms amenable to the physical requirements of a high-power radar. The implementation scheme is rather straightforward as demonstrated by the Matlab™ function provided in Table XI (note that this is a first-order implementation [36] and additional variants have also been developed [50,51]).

TABLE XI. MATLAB™ FUNCTION TO IMPLEMENT A FIRST-ORDER PCFM WAVEFORM

```
    % alpha: code of phase-shifts, bound between ±π
    % over: "over-sampling" with respect to 3 dB bandwidth, generally ≥ 2

function  s = PCFM(alpha,over)
    Len = length(alpha);          % length of code
    f = ones(over,1);        % define rectangular shaping filter
    f = f. / sum(f) ;        % normalize shaping filter to integrate to unity
    train = zeros (1,over*Len);        % define impulse train
    train(1:over:end) = alpha;        % weight impulse train with code values
    pfilt = filter(f,1,train);        % apply shaping filter to weighted impulse train
    phi = filter(1,[1 -1],pfilt);        % integrate response from shaping filter
    s = exp(j*phi);        % resulting complex baseband waveform
```

The primary waveform has been optimized according to the 'performance diversity' approach [37] to yield a peak sidelobe level (PSL) of –44.4 dB. The $K=4$ secondary waveforms were selected as the four waveforms having the lowest cross-correlation with the primary waveform (via (16)) from among a set of 10,000 randomly generated polyphase codes and subsequent PCFM implementation. These waveforms have peak cross-correlations of –16.6, –16.4, –16.2, and –16.1 dB and integrated cross-correlations of 0.9, 1.1, 1.0, and 1.1, for k = 1, 2, 3, and 4, respectively.

Since BT is well approximated by code length for PCFM [36], we use $N_{\text{code}}=100$. For $Q=64$ possible phase transitions drawn from a uniform sampling over the phase interval $[-\pi,\ \pi]$, the phase transition sequence can be expressed as

$$\alpha_n = 2\pi\left(\frac{q_n-1}{Q-1}\right)-\pi \tag{43}$$

with index $q_n \in [1, 2, \cdots, Q]$ such that $q=1$ corresponds to $\alpha=-\pi$ and $q=Q$ corresponds to $\alpha=+\pi$. For the waveforms used here, $f(t)$ is a rectangular shaping filter, the integration stage is implemented using a simple IIR filter with transfer function $H(z)=z/(z-1)$, and the waveforms are "over-sampled" by 5 with respect to their 3 dB bandwidth (see Table XI). Based on the conversion in (43), the indices for these five waveforms are listed in Table XII.

TABLE XII. PHASE TRANSITION INDICES q_n TO IMPLEMENT $BT = 100$ PCFM WAVEFORMS FOR USE IN MIMO AND SIMO μ-STAP SIMULATIONS

Primary waveform [1, 13, 12, 15, 18, 17, 20, 18, 20, 21, 21, 22, 22, 21, 23, 24, 23, 25, 23, 25, 24, 25, 26, 26, 27, 26, 27, 26, 28, 27, 28, 28, 28, 28, 29, 29, 29, 30, 30, 30, 31, 30, 30, 31, 31, 31, 32, 32, 32, 33, 32, 33, 33, 33, 33, 34, 33, 35, 35, 35, 35, 35, 35, 36, 35, 36, 37, 37, 37, 36, 38, 38, 39, 37, 40, 39, 38, 40, 39, 40, 41, 42, 40, 43, 40, 43, 43, 44, 43, 44, 44, 47, 46, 47, 46, 49, 49, 55, 52, 64]
Secondary waveform, k = 1 [28, 41, 45, 55, 4, 6, 59, 30, 45, 54, 22, 55, 8, 56, 27, 12, 25, 24, 5, 60, 31, 5, 25, 13, 1, 3, 64, 49, 46, 62, 10, 64, 9, 19, 6, 36, 31, 57, 54, 45, 48, 29, 1, 10, 45, 11, 30, 23, 9, 20, 62, 53, 64, 57, 29, 62, 6, 3, 63, 4, 61, 16, 9, 30, 15, 62, 42, 60, 56, 3, 35, 8, 50, 52, 58, 12, 33, 4, 2, 46, 60, 60, 13, 2, 43, 55, 52, 24, 63, 64, 48, 44, 10, 6, 28, 19, 45, 2, 34, 40]
Secondary waveform, k = 2 [35, 54, 58, 55, 31, 55, 44, 41, 55, 22, 43, 58, 33, 38, 26, 14, 59, 46, 11, 7, 22, 30, 24, 28, 60, 60, 2, 59, 50, 16, 39, 51, 50, 46, 59, 27, 47, 63, 29, 42, 9, 63, 18, 51, 53, 62, 59, 14, 1, 26, 1, 39, 50, 55, 42, 7, 38, 12, 36, 55, 6, 37, 62, 30, 52, 27, 3, 50, 2, 57, 64, 46, 23, 16, 26, 17, 31, 28, 6, 22, 23, 1, 63, 59, 8, 29, 54, 27, 37, 54, 37, 39, 1, 53, 44, 45, 17, 25, 1, 63]
Secondary waveform, k = 3 [22, 17, 28, 10, 53, 56, 37, 3, 52, 48, 5, 63, 21, 24, 20, 51, 17, 11, 42, 41, 58, 45, 10, 13, 27, 59, 7, 6, 2, 43, 53, 9, 2, 7, 8, 25, 62, 44, 17, 34, 45, 49, 12, 54, 38, 16, 11, 50, 53, 57, 15, 24, 42, 19, 7, 44, 1, 29, 4, 61, 44, 62, 42, 59, 60, 5, 29, 7, 27, 21, 15, 1, 21, 30, 1, 45, 26, 42, 57, 17, 8, 14, 18, 58, 2, 27, 10, 21, 52, 2, 12, 21, 50, 60, 25, 53, 35, 6, 12, 61]
Secondary waveform, k = 4 [41, 55, 24, 2, 21, 60, 16, 23, 6, 42, 44, 3, 44, 40, 20, 27, 37, 55, 34, 38, 61, 22, 31, 30, 50, 50, 54, 64, 60, 29, 44, 36, 2, 2, 7, 23, 19, 13, 26, 11, 47, 8, 14, 3, 14, 29, 9, 39, 7, 56, 1, 13, 2, 50, 41, 15, 46, 42, 26, 51, 4, 63, 53, 59, 59, 6, 29, 28, 58, 24, 30, 17, 40, 51, 12, 61, 2, 7, 14, 15, 11, 50, 15, 21, 2, 7, 64, 34, 31, 29, 14, 29, 6, 41, 60, 41, 55, 34, 21, 6]

REFERENCES

[1] S.D. Blunt, J. Jakabosky, J. Metcalf, J. Stiles, and B. Himed, “Multi-waveform STAP,” *IEEE Radar Conf.*, Ottawa, Canada, 29 Apr. – 3 May 2013.

[2] S.D. Blunt, J. Metcalf, J. Jakabosky, and B. Himed, “SINR analysis of multi-waveform STAP,” *IEEE Intl. Radar Conf.*, Lille, France, 13-17 Oct. 2014.

[3] J. Ward, “Space-time adaptive processing for airborne radar,” *Lincoln Lab Tech. Report*, TR-1015, Dec. 1994.

[4] W.L. Melvin, “A STAP overview,” *IEEE Aerospace & Electronic Systems Mag.*, vol. 19, no. 1, pp. 19-35, Jan. 2004.

[5] D.M. Boroson, “Sample size considerations for adaptive arrays,” *IEEE Aerospace & Electronic Systems*, vol. AES-16, no. 4, pp. 446-451, July 1980.

[6] K. Gerlach, “The effects of signal contamination on two adaptive detectors,” *IEEE Trans. Aerospace & Electronic Systems*, vol. 31, no. 1, pp. 297-309, Jan. 1995.

[7] W.L. Melvin, “Space-time adaptive radar performance in heterogeneous clutter,” *IEEE Trans. Aerospace & Electronic Systems*, vol. 36, no. 2, pp. 621-633, Apr. 2000.

[8] K. Gerlach and M.L. Picciolo, “Airborne/spacebased radar STAP using a structured covariance matrix,” *IEEE Trans. Aerospace & Electronic Systems*, vol. 39, no. 1, pp. 269-281, Jan. 2003.

[9] I.S. Reed, J.D. Mallett, and L.E. Brennan, “Rapid convergence rate in adaptive arrays,” *IEEE Trans. Aerospace & Electronic Systems*, vol. 10, no. 6, pp. 853-863, Nov. 1974.

[10] P. Chen, W.L. Melvin, and M.C. Wicks, “Screening among multivariate normal data,” *Journal of Multivariate Analysis*, vo. 69, no. 1, pp. 10-29, Apr. 1999.

[11] J.R. Guerci, “Theory and application of covariance matrix tapers for robust adaptive beamforming,” *IEEE Trans. Signal Processing*, vol. 47, no. 4, pp. 977-985, Apr. 1999.

[12] D.J. Rabideau and A.O. Steinhardt, “Improved adaptive clutter cancellation through data-adaptive training,” *IEEE Trans. Aerospace and Electronic Systems*, vol. 35, no. 3, pp. 879-891, July 1999.

[13] S.M. Kogon and M.A. Zatman, “STAP adaptive weight training using phase and power selection criteria,” *35th Asilomar Conf. Signals, Systems & Computers*, Pacific Grove, CA, pp. 98-102, Nov. 2001.

[14] G. Benitz, J.D. Griesbach, and C. Rader, “Two-parameter power-variable-training STAP,” *38th Asilomar Conf. Signals, Systems & Computers*, Pacific Grove, CA, pp. 2359-2363, Nov. 2004.

[15] T.M. Selee, K.F. Bing, and W.L. Melvin, “STAP application in mountainous terrain: challenges and strategies,” *IEEE Radar Conf.*, Atlanta, GA, pp. 824-829, May 2012.

[16] J.R. Roman, M. Rangaswamy, D.W. Davis, Q. Zhang, B. Himed, and J.H. Michels, “Parametric adaptive matched filter for airborne radar applications,” *IEEE Trans. Aerospace & Electronic Systems*, vol. 36, no. 2, pp. 677-692, Apr. 2000.

[17] R.S. Adve, T.B. Hale, and M.C. Wicks, “Practical joint domain localized adaptive processing in homogeneous and nonhomogeneous environments. Part 2: nonhomogeneous environments,” *IEE Proc. Radar, Sonar & Navigation*, vol. 147, no. 2, pp. 66-74, Apr. 2000.

[18] T.K. Sarkar, H. Wang, S. Park, R. Adve, J. Koh, K. Kim, Y. Zhang, M.C. Wicks, and R.D. Brown, “A deterministic least-squares approach to space-time adaptive processing (STAP),” *IEEE Trans. Antennas & Propagation*, vol. 49, no. 1, pp. 91-103, Jan. 2001.

[19] G.A. Fabrizio and M.D. Turley, “An advanced STAP implementation for surveillance radar systems,” *IEEE Workshop on Statistical Signal Processing*, Singapore, pp. 134-137, 6-8 Aug. 2001.

[20] K. Gerlach, “Outlier resistance adaptive matched filtering,” *IEEE Trans. Aerospace & Electronic Systems*, vol. 38, no. 3, pp. 885-901, July 2002.

[21] Y.-L. Wang, J.-W. Chen, Z. Bao, and Y.-N. Peng, “Robust space-time adaptive processing for airborne radar in nonhomogeneous environments,” *IEEE Trans. Aerospace & Electronic Systems*, vol. 39, no. 1, pp. 70-81, Jan. 2003.

[22] M.L. Picciolo and K. Gerlach, “Median cascaded canceller for robust adaptive array processing,” *IEEE Trans. Aerospace & Electronic Systems*, vol. 39, no. 3, pp. 883-900, July 2003.

[23] K. Gerlach, S.D. Blunt, and M.L. Picciolo, “Robust adaptive matched filtering using the FRACTA algorithm,” *IEEE Trans. Aerospace & Electronic Systems*, vol. 40, no. 3, pp. 929-945, July 2004.

[24] S.D. Blunt and K. Gerlach, “Efficient robust AMF using the FRACTA algorithm,” *IEEE Trans. Aerospace & Electronic Systems*, vol. 41, no. 2, pp. 537-548, Apr. 2005.

[25] W.L. Melvin and J.R. Guerci, “Knowledge-aided signal processing: a new paradigm for radar and other advanced sensors,” *IEEE Trans. Aerospace & Electronic Systems*, vol. 42, no. 3, pp. 983-996, July 2006.

[26] W.L. Melvin and G.A. Showman, “An approach to knowledge-aided covariance estimation,” *IEEE Trans. Aerospace & Electronic Systems*, vol. 42, no. 3, pp. 1021-1042, July 2006.

[27] S.D. Blunt, K. Gerlach, and M. Rangaswamy, “STAP using knowledge-aided covariance estimation and the FRACTA algorithm,” *IEEE Trans. Aerospace & Electronic Systems*, vol. 42, no. 3, pp. 1043-1057, July 2006.

[28] F. Gini, M. Rangaswamy, eds., *Knowledge Based Radar Detection, Tracking, and Classification*, John Wiley & Sons, Inc., 2008.

[29] E. Aboutanios and B. Mulgrew, “Hybrid detection approach for STAP in heterogeneous clutter,” *IEEE Trans. Aerospace & Electronic Systems*, vol. 46, no. 3, pp. 1021-1033, July 2010.

[30] O. Besson and S. Bidon, “Adaptive processing with signal contaminated training samples,” *IEEE Trans. Signal Processing*, vol. 61, no. 17, pp. 4318-4329, Sept. 2013.

[31] A. Steinhardt and J. Guerci, “STAP for radar: what works, what doesn’t and what’s in store,” *IEEE Radar Conf.*, Philadelphia, PA, pp. 469-473, 26-29 Apr. 2004.

[32] M. Wicks, E. Mokole, S. Blunt, R. Schneible, and V. Amuso, eds., *Principles of Waveform Diversity and Design*, SciTech Publishing, 2010.

[33] U. Pillai, K.Y. Li, I. Selesnick, and B. Himed, *Waveform Diversity: Theory & Applications*, McGraw-Hill, 2011.

[34] F. Gini, A. De Maio, and L. Patton, eds., *Waveform Design and Diversity for Advanced Radar Systems*, IET, 2012.

[35] S.D. Blunt and E.L. Mokole, “An overview of radar waveform diversity,” *IEEE AES Systems Magazine*, Oct. 2016.

[36] S.D. Blunt, M. Cook, J. Jakabosky, J. de Graaf, E. Perrins, “Polyphase-coded FM (PCFM) radar waveforms, part I: implementation,” *IEEE Trans. Aerospace & Electronic Systems*, vol. 50, no. 3, pp. 2218-2229, July 2014.

[37] S.D. Blunt, J. Jakabosky, M. Cook, J. Stiles, S. Seguin, and E. Mokole, "Polyphase-coded FM (PCFM) radar waveforms, part II: optimization," *IEEE Trans. Aerospace & Electronic Systems*, vol. 50, no. 3, pp. 2230-2241, July 2014.

[38] M.A. Richards, J.A. Scheer, and W.A. Holm, *Principles of Modern Radar: Basic Principles*, SciTech, 2010, Sect. 16.5.

[39] F. Daum and J. Huang, "MIMO radar: snake oil or good idea?," *IEEE Aerospace & Electronic Systems Mag.*, pp. 8-12, May 2009.

[40] G.J. Frazer, Y.I. Abramovich, and B.A. Johnson, "Multiple-input multiple-output over-the-horizon radar: experimental results," *IET Radar, Sonar & Navigation*, pp. 290-303, 2009.

[41] R.J. Riddols, M. Ravan, and R.S. Adve, "Canadian HF over-the-horizon radar experiments using MIMO techniques to control auroral clutter," *IEEE Intl. Radar Conf.*, Washington, DC, pp. 718-723, 10-14 May 2010.

[42] S. Coutts, K. Cuomo, J. McHarg, F. Robey, and D. Weikle, "Distributed coherent aperture measurements for next generation BMD radar," *IEEE Sensor Array & Multichannel Workshop*, Waltham, MA, pp. 390-393, 12-14 July 2006.

[43] B. Cordill, J. Metcalf, S.A. Seguin, D. Chatterjee, and S.D. Blunt, "The impact of mutual coupling on MIMO radar emissions," *IEEE Intl. Conf. on EM in Advanced Applications*, pp. 644-647, 12-16 Sept. 2011.

[44] G. Babur, P.J. Aubry, F. Le Chevalier, "Antenna coupling effects for space-time radar waveforms: analysis and calibration," *IEEE Trans. Antennas & Propagation*, vol. 62, no. 5, pp. 2572–2586, May 2014.

[45] J.S. Bergin, C.M. Teixeira, and P.M. Techau, "Multi-resolution signal processing techniques for airborne radar," *IEEE Radar Conf.*, pp. 277-282, Philadelphia, PA, 26-29 Apr. 2004.

[46] G.A. Akers and J.M. Stiles, "An approach to ground moving target indication (GMTI) using multiple resolutions of the clutter covariance matrix," *IEEE Radar Conf.*, Pasadena, CA, 4-8 May 2009.

[47] J. Billingsley, A. Farina, F. Gini, M. Greco, and L. Verrazzani, "Statistical analyses of measured radar ground clutter data," *IEEE Trans. Aerospace & Electronic Systems*, vol. 35, no. 2, pp. 579-593, Apr. 1999.

[48] J.G. Metcalf, K.J. Sangston, M. Rangaswamy, S.D. Blunt, and B. Himed, "A new method of generating multivariate Weibull distributed data," *IEEE Radar Conf.*, Philadelphia, PA, May 2016.

[49] R. Bose, A. Freedman, and B. Steinberg, "Sequence CLEAN: a modified deconvolution technique for microwave images of contiguous targets," *IEEE Trans. Aerospace & Electronic Systems*, vol. 38, no. 1, pp. 89-97, Jan. 2002.

[50] J. Jakabosky, S.D. Blunt, and B. Himed, "Optimization of "over-coded" radar waveforms," *IEEE Radar Conf.*, Cincinnati, OH, 19-23 May 2014.

[51] P.S. Tan, J. Jakabosky, J.M. Stiles, and S.D. Blunt, "On higher-order representations of polyphase-coded FM radar waveforms," *IEEE Intl. Radar Conf.*, Washington, DC, 11-15 May 2015.